Transplantation Elicits a Clonally Diverse CD8$^+$ T Cell Response that is Comprised of Potent CD43$^+$ Effectors

Gregory A. Cohen[1], Melissa A. Kallarakal[1], Sahana Jayaraman[1], Francis I. Ibukun[1], Katherine P. Tong[2], Linda D. Orzolek[3], H. Benjamin Larman[1], Scott M. Krummey[1]*

[1]Department of Pathology, Johns Hopkins School of Medicine, Baltimore, MD

[2]Emory Transplant Center, Emory University School of Medicine, Atlanta, GA

[3]Department of Molecular Biology and Genetics, Johns Hopkins School of Medicine, Baltimore, MD

*Correspondence: skrumme1@jhmi.edu

Keywords: effector CD8$^+$ T cells, alloimmunity, costimulation blockade

Character Count: 37,638

SUMMARY

$CD8^+$ T cells mediate acute rejection of allografts, which threatens the long-term survival of transplanted organs. The factors that govern differentiation of graft-directed effector $CD8^+$ T cells could lead to targeted approaches to limit acute rejection. Using MHC Class I tetramers, we found that allogeneic $CD8^+$ T cells were present at an elevated precursor frequency in naïve mice, only modestly increased in number after grafting, and maintained high T cell receptor diversity throughout the immune response. While antigen-specific effector $CD8^+$ T cells poorly express the canonical effector marker KLRG-1, expression of the activated glycoform of CD43 defined potent effectors after transplantation. Activated $CD43^+$ effector T cells maintained high expression of ICOS in the presence of CTLA-4 Ig, and dual CTLA-4 Ig/anti-ICOS treatment prolonged graft survival. These data demonstrate that graft-specific $CD8^+$ T cells have a distinct response profile relative to anti-pathogen $CD8^+$ T cells, and that CD43 and ICOS are critical surface receptors that define potent effector $CD8^+$ T cell populations that form after transplantation.

INTRODUCTION

Activation of $CD8^+$ T cells relies on the recognition of cognate antigen in the presence of both coreceptor signaling and the local cytokine milieu (Chung et al., 2021; Ford, 2016; Jameson and Masopust, 2018). The balance of these factors shapes the magnitude and character of the $CD8^+$ T cell response. In transplantation, $CD8^+$ T cells can respond to allogeneic antigen presented on donor MHC Class I proteins and mediate tissue damage (Callemeyn et al., 2021; Felix et al., 2007). Recent clinical studies have highlighted that the occurrence of acute rejection has cumulative and detrimental effects on the long-term survival of transplanted organs (Cherukuri et al., 2021; Cole et al., 2008; Meier-Kriesche et al., 2000).

Activated T cells undergo several well-established phenotypic changes that distinguish them from quiescent naïve $CD8^+$ T cells. The majority of the work underlying these paradigms has been performed in infection models, which present distinct profiles of inflammation and antigen relative to transplanted organs (Braza et al., 2016; Colvin et al., 2017; Dwyer and Turnquist, 2021). The canonical phenotype of an effector $CD8^+$ T cell, $CD44^{hi}CD62L^{lo}$, does not specifically distinguish the actively responding graft-specific $CD8^+$ T cells among the larger pool of previously activated cells. Expression of the surface receptor KLRG-1 is also used to identify actively responding effector $CD8^+$ T cells relative to memory precursor cells (Herndler-Brandstetter et al., 2018a; Joshi et al., 2007; Sarkar et al., 2008). However, KLRG-1 expression is not functionally required for the effector function of $CD8^+$ T cells nor is it induced after all types of priming *in vivo* (Bozeman et al., 2018; Joshi et al., 2007). Thus, in order to more granularly understand anti-graft $CD8^+$ T cell responses and develop strategies to target the allogeneic response, a deeper understanding of the differentiation program of post-graft $CD8^+$ T cells is needed.

Due to the technical difficulties associated with identifying allogeneic peptide epitopes, the $CD8^+$ T cell response is typically evaluated by using either TCR transgenic mice (e.g. OT-I/OVA) or evaluating the “bulk” pool of activated $CD8^+$ T cells. Both approaches sacrifice potential insights

gained by assessing the acutely responding antigen-specific T cell clones in the context of physiologic antigen levels, precursor frequency, clonal competition, and inflammatory signals. MHC tetramers have provided a tremendous advance in the ability to identify and track antigen-specific $CD8^+$ T cell responses to pathogens and model antigens (Haluszczak et al., 2009; Jenkins and Moon, 2012; Kotturi et al., 2008; Obar et al., 2008). However, the use of MHC tetramers to study allogeneic T cells has been limited due to the technical challenges of identifying appropriate epitopes from across the proteome.

We sought to develop the use of MHC tetramers in a fully allogeneic transplant model by taking advantage of elegant work performed in the characterization of the allogeneic 2C TCR transgenic mouse model several decades ago (Chen et al., 2003; Sykulev et al., 1994a; Udaka et al., 1992). We found that MHC tetramers of an H-$2L^d$ restricted epitope for a ubiquitously expressed metabolic enzyme defined a population of $CD8^+$ T cells in H-2^b C57Bl/6 mice. This approach allowed us to directly study the $CD8^+$ T cell response to fully allogeneic H-2^d grafts and characterize the differentiation of effector populations in the context of physiologic antigen and inflammation. Here we report the characteristics of the $CD8^+$ T cell response to allogeneic antigen, including the clonal features of antigen-specific alloreactive $CD8^+$ T cells, and the emergence of a potent population of effector $CD8^+$ T cells that express the surface receptor CD43 after grafting.

RESULTS

MHC Class I tetramer can be used to identify L^d $QL9^+$ $CD8^+$ T cells in naïve C57Bl/6 mice

Relatively few allogeneic epitopes have been identified in the fully allogeneic Balb/c (H-2^d) to C57Bl/6 (H-2^b) transplant model. The alloreactive 2C TCR recognizes H-$2L^d$ restricted peptides for the self-peptide α-ketoglutarate dehydrogenase(Chen et al., 2003; Sykulev et al., 1994a; Udaka et al., 1992), thus representing a directly presented allogeneic epitope. We hypothesized that MHC tetramers of this H-$2L^d$ restricted epitope could be used to identify endogenous alloreactive $CD8^+$ T cells. In order to reliably detect rare $CD8^+$ T cells, we incubated single cell suspensions of secondary lymphoid organs with L^d QL9 tetramers and enriched with magnetic beads specific for the fluorophore(s) of the tetramer **(Figure 1A)**(Moon et al., 2007). This approach results in a tetramer enriched (column "bound") and bulk $CD8^+$ (column "unbound") fractions of cells for analysis.

In naïve C57Bl/6 mice, we detected a population of L^d QL9 tetramer binding cells using PE and APC tetramers **(Figure 1B)**. Using this approach, we identified L^d QL9-specific $CD8^+$ T cells in the spleen and lymph nodes (mean 4,994 and 1,199 cells/tissue, respectively**; Figure 1C-D)**. Tetramer binding was specific, as no L^d QL9 binding cells were found in OT-I RAG1 KO mice **(Figure 1C)**. The phenotype of L^d QL9 binding $CD8^+$ T cells was largely $CD44^{lo}CD62L^{hi}$, similar to the bulk $CD8^+$ T cell population in naive **(Figure 1E)**. We found that the precursor frequency of K^b OVA and D^b LCMV gp33-specific $CD8^+$ T cells, while consistent with prior publications (Jenkins and Moon, 2012), were significantly lower than that of L^d QL9 $CD8^+$ T cells **(Figure 1F-G)**. Thus, the L^d QL9 tetramer specifically binds to a population of naïve $CD8^+$ T cells that appear to be at a relatively elevated precursor frequency compared with other T cell populations.

L^d $QL9^+$ $CD8^+$ T cells become activated and proliferate after H-2^d Balb/c skin grafts

Having established that a population of H-2^b C57Bl/6 $CD8^+$ T cells recognize L^d QL9 tetramers in naïve mice, we next wanted to evaluate whether L^d $QL9^+$ $CD8^+$ T cells respond when presented with allogeneic H-$2L^d$ antigen-expressing tissue. We grafted skin from H-2^d Balb/c mice onto C57Bl/6 mice and assessed tetramer binding $CD8^+$ T cells **(Figure 2A)**. We found that a significant portion of L^d $QL9^+$ $CD8^+$ T cells became $CD44^{hi}$ on day 10 after skin grafting in the draining lymph nodes and spleen **(Figure 2B)**, indicative of priming after exposure to cognate antigen. The absolute number of $CD44^{hi}$ L^d QL9 tetramer binding cells increased on day 10 in both the draining lymph nodes and spleen **(Figure 2C)**, representing an average 10-fold increase in the draining lymph node and 6.1-fold in the spleen **(Figure 2D)**.

In order to assess whether the phenotypic and cell number changes reflected a proliferative response in L^d QL9-specific $CD8^+$ T cells, we stained cells for Ki67 in order to assess recent and active proliferation after Balb/c skin grafting. We found that in both the draining lymph node and spleen, the frequency of $Ki67^+$ cells increased by day 7, and peaked on day 10 relative to naïve $CD8^+$ T cells **(Figure 2E).** At day 10 post-transplant, nearly all of the L^d $QL9^+$ $CD44^{hi}$ $CD8^+$ T cells were $Ki67^+$ in both the draining lymph nodes and spleen **(Figure 2E)**. The frequency of $Ki67^+$ $CD8^+$ T cells also peaked in the bulk $CD8^+$ T cell population at day 10 **(Figure S1)**. Thus, as measured by both absolute numbers and $Ki67^+$ frequency, L^d QL9 tetramer binding $CD8^+$ T cells respond to endogenously presented antigen in Balb/c skin grafts.

Graft-specific $CD8^+$ T cells maintain clonal diversity during the peak effector response

Given that the L^d QL9-specific $CD8^+$ T cells are found at an elevated precursor frequency relative to $CD8^+$ T cell populations specific for non-transplant antigens **(Figure 1G)**, yet underwent a relatively modest fold expansion after grafting **(Figure 2D)**, we sought to evaluate the clonal dynamics of this antigen-specific population. We used a multiplexed *TCRB* sequencing platform in order to evaluate the anti-graft $CD8^+$ T cell response in naïve and effector graft-specific $CD8^+$ T cells. To identify a graft-specific *TCRB* signature, we sequenced FACS-sorted naïve $CD44^{lo}$ L^d

QL9$^+$ T cells from naive mice and effector CD44^{hi} L^d QL9$^+$ T cells from mice on day 10 post-Balb/c skin graft to compare with bulk (L^d QL9$^-$) CD8$^+$ T cells sorted into CD44^{lo} naïve and CD44^{hi} effector populations **(Figure 3A).**

We found that CD44^{hi} L^d QL9$^+$ T cells had significantly less population diversity versus naïve CD44^{lo} L^d QL9$^+$ T cells, consistent with greater oligoclonality after grafting **(Figure 3B).** In order to evaluate the dynamics of clones that were enriched in the CD44^{hi} L^d QL9$^+$ population, we used the TCRdist package, which identifies biochemically similar CDR3 sequences called meta-clonotypes, in antigen-specific T cell populations evaluated in comparison with background populations (Dash et al., 2017). We identified 43 meta-clonotypes that were enriched over background in our samples **(Table S1)**. Compared with the naïve L^d QL9$^+$ population, we found that a greater number of the post-graft CD44^{hi} L^d QL9$^+$ meta-clonotypes were found to have medium expansion, large expansion, and hyper-expansion frequencies **(Figure 3C)**. Interestingly, clones recovered from within the skin grafts on day 10 remained relatively polyclonal, and all grafts contained meta-clonotypes **(Figure 3D)**.

We next evaluated the representation of meta-clonotypes across individual mice, and found that 13 meta-clonotypes were convergent, which we defined as present in 75% or more of the individual mice CD44^{hi} L^d QL9$^+$ populations **(Figure 3E)**. The defining amino acid sequences of these meta-clonotypes varied, although there was a preference for a glycine at position 5 and/or 6, which was present in 8 of 13 of the convergent meta-clonotypes. We evaluated the expression of the convergent meta-clonotypes and found that they were enriched in the L^d QL9$^+$ CD8$^+$ T cells at day 10 post-graft relative to naïve populations **(Figure 3F).** In each mouse, at least one of the convergent meta-clonotypes was present **(Figure 3G-H)**. However, we did not find an increased number of convergent meta-clonotypes in the unsorted peripheral blood or skin grafts **(Figure 3G-H)**. Thus, these data demonstrate that after transplantation, CD8$^+$ T cells responding to a single allogeneic antigen maintain high clonal diversity. However, there may be biochemical properties that govern CD8$^+$ T cell recognition of allogeneic antigen.

1

2 **A low frequency of CD8$^+$ T$_{EFF}$ express KLRG-1$^+$ after grafting**

3 A significant goal in transplantation is to identify acutely responding T cells in order to
4 monitor the risk for, or presence of, acute cellular graft rejection. In order to understand the
5 function of graft-specific effector CD8$^+$ T cells, we evaluated the phenotypic profile of L^d QL9$^+$
6 effector CD8$^+$ T cells (T$_{EFF}$), as defined by CD44^{hi} status. We first evaluated the expression of
7 CXCR3 and CD62L, two surface receptors that have been shown to be important for post-
8 infection T$_{EFF}$ function. We found that nearly all L^d QL9$^+$ and bulk CD8$^+$ T cells became CXCR3$^+$
9 at day 10 and remained stable to a memory timepoint **(Figure 4A-C)**. About half of these CXCR3$^+$
10 T$_{EFF}$ lost CD62L expression, and this frequency of CD62L^{lo} cells was also stable from day 10-42
11 after skin grafting. Thus, while these markers are useful for identifying antigen-experienced CD8$^+$
12 T cells after transplantation, they do not delineate acutely responding effectors.

13 The early CD8$^+$ T cell response is often defined by the reciprocal expression of the CD127
14 (IL-7Rα) and KLRG-1 receptors. In the first 1-2 weeks after infection, a significant portion (50-
15 70%) of T$_{EFF}$ transiently downregulate CD127 and become KLRG-1$^+$, and these cells are short-
16 lived and display potent effector functions(Herndler-Brandstetter et al., 2018b; Joshi et al., 2007;
17 Milner et al., 2020). We assessed the expression of CD127 and KLRG-1 among L^d QL9$^+$ T$_{EFF}$
18 after grafting in both the spleen and draining lymph nodes. In response to a Balb/c skin graft, a
19 low frequency of CD127^{lo}KLRG1$^+$ T$_{EFF}$ cells were induced among L^d QL9$^+$ and bulk CD8$^+$ T cells
20 in the spleen, with a peak frequency at day 10 that declined precipitously at day 21 and 42 **(Figure**
21 **4D-E)**. In the draining lymph node, a similarly low frequency of KLRG-1$^+$ T$_{EFF}$ were found **(Figure**
22 **4F-G)**. Thus, these data show that among graft-specific L^d QL9$^+$ cells after transplantation, KLRG-
23 1 expression does not define an abundant population of acutely responding T$_{EFF}$.

24

25 **Expression of the activated CD43 glycoform is increased on a population of CD8$^+$ T$_{EFF}$ after**
26 **grafting**

To better characterize the phenotypes of the $CD8^+$ T_{EFF} cells after grafting, we analyzed a high-parameter flow cytometry panel with canonical costimulatory and activation using dimensionality reduction analysis. We evaluated L^d $QL9^+$ and bulk $CD8^+$ T cells on day 0, 10, 21, and 42 after Balb/c skin grafting by clustering these populations with FlowSOM and ConsensusClusterPlus and visualized with uniform manifold approximation and projection (UMAP) dimensionality reduction **(Figure 5A-C)**. We evaluated the frequency of clusters and found four clusters that were enriched on day 10 relative to the other timepoints, and three clusters that were enriched on both day 21 and 42 **(Figure 5B-C)**. We further evaluated day 10 enriched clusters, as these fit the profile of a short-lived effector population. All four Day 10 Clusters were $CD44^{hi}$, $Ki67^+$, $CXCR3^{hi}$ and KLRG-1^- **(Figure 5D)**. Interestingly, these clusters varied most in expression of CD62L and the activated glycoform of CD43 (identified by the antibody clone 1B11). While Day 10 Clusters 1 and 2 were $CD62L^{hi}CD43^-$, Cluster 3 was $CD62L^{lo}CD43^-$, and Cluster 4 was $CD62L^{lo}CD43^+$ (**Figure 5D).** Thus, these two surface receptors appear to represent dynamic populations within the T_{EFF} pool after grafting. In order to evaluate the expression of CD62L and CD43 after grafting, we performed manual gating on L^d $QL9^+$ and bulk $CD8^+$ T_{EFF}. We found that the frequency of $CD62L^{lo}CD43^+$ T_{EFF} increased at day 10 and 21 and were decreased at a memory day 42 timepoint **(Figure 5E)**. Thus, activated CD43 expression defines a population of $CD62L^{lo}$ T_{EFF} that appears acutely after grafting and declines over time, fitting the kinetic profile of an acutely responding $CD8^+$ T_{EFF} population.

$CD43^+$ $CD8^+$ T_{EFF} display potent effector functions relative to $CD43^-$ T_{EFF} populations.

CD43 is a transmembrane receptor that has been shown to impact intracellular signaling cascades, apoptosis, and T cell trafficking. However, the role of activated CD43 expression on $CD8^+$ T cells has not been evaluated. Thus, we next sought to assess whether $CD43^+$ T_{EFF} displayed competent effector functions relative to $CD43^-$ T_{EFF} populations. We grafted C57Bl/6 mice with Balb/c skin and assessed $CD8^+$ T cells during the peak effector response (day 10-14;

Figure 6A). We found that among the L^d $QL9^+$ cells, $CD43^+$ T_{EFF} expressed significantly higher levels of both Granzyme B and T-Bet as compared with $CD62L^{hi}$ or $CD62L^{lo}$ $CD43^-$ T_{EFF} populations **(Figure 6B-C)**. We assessed the capacity of these populations for cytokine production by stimulating $CD45.1^+$ T_{EFF} *ex vivo* with Balb/c splenocytes, and found that nearly all of the IFN-γ and TNF-α was produced by $CD43^+$ T_{EFF}, and that the majority of these cells were double producers **(Figure 6D)**.

We wanted to assess whether the effector phenotype corresponded with an enhanced potency to mediate graft rejection *in vivo*. To isolate the impact of CD43 on T_{EFF}, we FACS-sorted $CD44^{hi}CD8^+$ T cells into $CD43^+$ and $CD43^-$ T_{EFF} ($CD62L^{lo}$) on day 10-14 and adoptively transferred $9x10^4$ cells into C57Bl/6 mice who were subsequently grafted with Balb/c skin. We found that the $CD43^+$ T_{EFF} group rejected skin grafts with significantly faster kinetics than $CD43^-$ T_{EFF} group **(Figure 6E-F)**, demonstrating the impact of $CD43^+$ T_{EFF} to mediate potent graft rejection. Overall, these data demonstrate that $CD43^+$ T_{EFF} are a potent population of effector $CD8^+$ T cells *in vivo*.

Activated CD43 expression is induced by antigen and Type I interferon.

Our data show that activated CD43 is induced after grafting *in vivo*, which entails exposure to both allogeneic antigen and inflammatory cytokines. We questioned whether inflammatory cytokines alone drive the expression of activated CD43 during T cell priming. Multiple studies have demonstrated that pathogenic inflammation on the development and function of $CD8^+$ T cell populations(Joshi et al., 2007; Richer et al., 2015). We activated OT-I T cells *in vitro* in the presence of individual inflammatory cytokines **(Figure 6G)**. We used CellTrace Violet to assess the proliferation status of cells in culture. We included expression of Nur77, an orphan nuclear receptor whose expression level reflects the cumulative strength of antigen stimulation(Krummey et al., 2016; Moran et al., 2011), as a control for the overall level of activation of the cells in the presence of cytokines. We found that antigen stimulation alone induced CD43 and Nur77 expression **(Figure 6H)**. The TLR9 agonist CpG, which has been shown to induce CD43 (1B11)

expression(Nolz and Harty, 2014), increased CD43 expression further than antigen stimulation alone. Among inflammatory cytokines, we found that only IFN-α induced CD43 expression, while IFN-γ, IL-15, and IL-12 did not have an effect versus antigen stimulation alone **(Figure 6H)**. The expression of Nur77 was not significantly impacted by the provision of any inflammatory cytokine. These results demonstrate that CD43 (1B11) expression is enhanced by antigen and can be augmented by Type I IFN mediated signaling.

Costimulation blockade with CTLA-4 Ig does not inhibit CD8$^+$ T cells.

Costimulation blockade with CTLA-4 Ig or a biochemical derivative is used to treat autoimmune disease and to prevent transplant rejection in kidney transplant patients. In transplant patients, CTLA-4 Ig is associated with acute T cell mediated rejection, and pre-clinical studies have shown that CD8$^+$ T cells are relatively resistant to CTLA-4 Ig (Crepeau and Ford, 2017; Ford et al., 2007; Liu et al., 2014). We next evaluated the impact of CTLA-4 Ig on CD43$^+$ T_{EFF} relative to other T_{EFF}. We treated mice with CTLA-4 Ig in comparison to a control untreated group and analyzed CD8$^+$ T cells on day 10 after grafting with Balb/c skin grafts **(Figure 7A)**. Consistent with prior studies, we found that CTLA-4 Ig reduced the proliferation of effector CD4$^+$ T cells but did not restrain CD8$^+$ effector T cell populations **(Figure S2)**.

In order to evaluate the phenotype of CD8$^+$ T cells in the presence of CTLA-4 Ig, we performed UMAP and clustering analysis of L^d QL9$^+$ and bulk CD8$^+$ T cells in treated and control mice **(Figure 7B)**. We found four clusters that were CD44^{hi} T_{EFF} and evaluated the expression of costimulation receptors, activation markers, and functional markers **(Figure 7B-D)**. CD44^{hi} Clusters 2 and 3 had high CD43 (1B11) expression, and were also CD62L^{lo}, CXCR3^{hi}, and Ki67$^+$. Interestingly, both had high expression of the costimulation receptor ICOS **(Figure 7D)**. Using manual gating, we evaluated whether the frequency of CD62L and CD43 T_{EFF} was impacted by CTLA-4 Ig treatment, and found that all three populations were maintained at similar frequencies

at day 10 between groups **(Figure 7E)**. We next evaluated ICOS expression on CD43 vs CD62L T_{EFF}, and found that ICOS expression was almost exclusively found on $CD62L^{lo}CD43^{+}$ T_{EFF} **(Figure 7F)**. In order to assess whether ICOS costimulation provisioned functional signals in the context of graft rejection, we assessed the impact of ICOS blockade in combination with CTLA-4 Ig treatment. We found that anti-ICOS prolonged graft survival versus CTLA-4 Ig alone **(Figure 7G)**. Thus, ICOS represents a functional costimulation target that can be used to inhibit CTLA-4 Ig resistant $CD8^{+}$ T cells.

DISCUSSION

CD8$^+$ T cells are thought to respond to allogeneic antigen primarily through the direct antigen presentation pathway, in which donor MHC complexed with ubiquitously expressed self peptides bind to host CD8$^+$ T cells (Harper et al., 2015; Siu et al., 2018). Burrack et al recently used MHC Class II tetramers to show that CD4$^+$ T cells can respond to directly presented allogeneic antigen in a mouse model of skin grafting (Burrack et al., 2018), but allogeneic CD8$^+$ T cells have not been studied using a similar approaches (Young et al., 2017). In this study, we build upon several elegant studies by Eisen and colleagues to study the CD8$^+$ T cell response directed against the H-2L^d complexed with the self-peptide QL9. While this early work defined the biochemistry of the 2C TCR binding with L^d QL9 *in vitro* (Chen et al., 2003; Sykulev et al., 1994a, 1994b, 1996; Udaka et al., 1992, 1996), the *in vivo* immune CD8+ T cell response directed at L^d QL9 has not been evaluated.

Thus, we sought to use MHC Class I tetramer enrichment approach to study L^d QL9-specific CD8$^+$ T cells. We found that at the peak of the immune response, the majority of L^d QL9$^+$ T cells become CD44^{hi} and nearly all CD44^{hi} L^d QL9$^+$ T cells are Ki67$^+$, providing strong evidence that the tetramer binding T cells recognize endogenously presented L^d QL9 on graft tissue. While the QL9 peptide is a single amino acid extension of the parent 2C peptide, prior studies investigating the peptides recognized by the 2C TCR speculated that the QL9 was not detected on donor antigen-presenting cells due to technical limitations of peptide sequencing in acidic conditions (Chen et al., 2003; Sykulev et al., 1994).

We found that the precursor frequency for L^d QL9$^+$ T cells is elevated compared with K^b OVA and D^b LCMV gp33, as well as the published frequencies of other pathogen-specific antigens (Haluszczak et al., 2009; Jenkins and Moon, 2012; Kotturi et al., 2008; Obar et al., 2008). Prior studies estimating the precursor frequency of alloreactive T cells have relied on a wide variety of techniques, including *in vitro* stimulation for proliferation or cytokine production, and have relied

on memory-containing T cell populations and/or expanded T cell lines (Amir et al., 2010; Felix et al., 2007; Heeger et al., 1999; Macedo et al., 2009; Suchin et al., 2001). Thus, our findings using an MHC tetramer to directly visualize epitope-specific $CD8^+$ T cells significantly strengthens the knowledge about the precursor frequency of alloimmunity gained from these prior studies.

Our results provide a model in which alloreactive $CD8^+$ T cells exist at a high precursor frequency but undergo relatively weak clonal expansion. Consistent with this, *TCRB* sequencing of the L^d QL9-specific CD8+ T cell response reveals a highly diverse response at the clonal level. While we identified biochemically similar group of convergent meta-clonotypes that expanded after grafting, the anti-graft $CD8^+$ T cell response remained diverse between individual animals. Interestingly, while we observed that the meta-clonotypes were present in graft tissue, the graft-infiltrating response was not dominated by the convergent clones at day 10 post-graft. Future studies are needed to gain a better understanding of the clonal properties and kinetics of the $CD8^+$ T cell infiltration into graft.

In contrast to pathogen-specific $CD8^+$ T cell responses at acute timepoints, we found that very few effector $CD8^+$ T cells expressed KLRG-1 after grafting. This highlights that the allogeneic priming environment has phenotypic consequences in shaping $CD8^+$ T cell responses, and led us to carefully evaluate the post-graft $CD8^+$ T cell programming. Using a high-parameter flow cytometry panel to evaluate activation, costimulation, and proliferation markers, we found that a subset of L^d $QL9^+$ T_{EFF} express the activated glycoform of CD43 (1B11 clone). The frequency $CD43^+$ T_{EFF} increased acutely after transplant and these cells were potently cytotoxic relative to $CD43^-$ T_{EFF} populations.

CD43 is a transmembrane receptor with recognized intracellular signaling and adhesion functions (Mody et al., 2007; Onami et al., 2002; Sperling et al., 1995). CD43 is uniformly high on T cells, but a larger activated glycoform, defined by the 1B11 epitope, is selectively expressed in certain contexts (Clark and Baum, 2012). Studies evaluating the role of CD43 in disease models have found varying and sometimes conflicting consequences. CD43 deficient $CD8^+$ T cells have

been found to undergo a decreased rate of apoptosis during the contraction phase of the response to a virus (Onami et al., 2002), but including increased levels of apoptosis in a model of sepsis (Fay et al., 2018). Multiple studies have shown that CD43 is critical for trafficking into peripheral tissues (Cannon et al., 2011; Ford and Evavold, 2006; Ford et al., 2003; Mody et al., 2007; Onami et al., 2002). Of note, the majority of studies have evaluated the function of CD43 sufficient versus strains, less is known about the functional impact of CD43 1B11 glycoform expression on T cells. Future studies will be needed to evaluate the importance of CD43 1B11 expression on the function of T_{EFF} in the context of transplant, including the ability to traffic within secondary lymphoid tissue and into allografts.

We evaluated antigen-specific T_{EFF} in the presence of costimulation blockade with CTLA-4 Ig, and found that the costimulatory receptor ICOS is selectively expressed on $CD43^+$ T_{EFF}. Blockade of ICOS prolonged graft survival, indicating that ICOS plays a functional role in the presence of CTLA-4 Ig treatment. ICOS has been implicated as an important costimulatory receptor in multiple T cell subsets, and was recently shown to be important for the formation of resident memory $CD8^+$ T cells (Peng et al., 2022). ICOS is attractive as a therapeutic target because it is selectively and transiently upregulated on $CD43^+$ T_{EFF}, and thus represents a potentially selective way to inhibit allogeneic $CD8^+$ T cells during rejection. Currently, ICOS blocking agents are in pre-clinical development for multiple diseases (Adom et al., 2020; Solinas et al., 2020).

Overall, by using a novel MHC tetramer-based approach, this study provides new insight into the characteristics of the alloimmune $CD8^+$ T cell response, including the identification of a potent T_{EFF} phenotype. Future studies are needed to investigate the translational potential of these findings to inhibit graft-specific $CD8^+$ T cells in transplant patients.

ACKNOWLEDGEMENTS

We thank members of the Ford Lab and the Immunology Division of the Department of Pathology at Johns Hopkins for helpful discussions. We appreciate Hao Zhang and the Bloomberg School of Public Health Flow Cytometry and Cell Sorting Core for excellent cell sorting, and the NIH Tetramer Core Facility for tetramer reagents and technical advice. This work was supported by K99/R00 NIAID AI46271 (S.M.K) and the Transplant Immunology Research Network Fellowship Grant (S.M.K.).

AUTHOR CONTRIBUTIONS

Conceptualization, S.M.K., H.B.L., G.A.C., S.J.; methodology, S.M.K., G.A.C., H.B.L., S.J.; formal analysis, S.M.K., G.A.C., S.A.J., H.B.L.; investigation, S.M.K., G.A.C., M.A.K., S.J., F.I.I., K.P.T., L.A.O.; writing, S.M.K., G.A.C., S.J.; visualization, S.M.K., G.A.C.; supervision, S.M.K., H.B.L.

DECLARATION OF INTEREST

The authors declare no competing interests.

FIGURE LEGENDS

Figure 1. H-2L^d QL9 tetramers identify a population of naive CD8$^+$ T cells at elevated precursor frequency. (A) Single cell suspensions of lymph node or spleen tissue were incubated with MHC Class I tetramers, and enriched using magnetic beads specific for the tetramer fluorophores, creating column bound tetramer-enriched and unbound bulk CD8$^+$ T cell fractions for analysis. (B) Representative flow cytometry plots and summary data depicting the frequency of CD8$^+$ T cells binding to L^d QL9 PE and L^d QL9 APC tetramers in the bound and unbound fractions. (C) Representative flow cytometry plots of L^d QL9 tetramer staining in naive C57Bl/6 spleen, C57Bl/6 lymph nodes, or OT-I RAG1$^{-/-}$ spleen. (D) Absolute numbers of L^d QL9 tetramer binding CD8$^+$ T cells in the lymph nodes and spleen of naive C57Bl/6 mice. (E) Representative flow cytometry plots and summary data depicting the phenotype of L^d QL9 tetramer binding CD8$^+$ T cells in the lymph nodes and spleen. (F) Representative flow cytometry plots of D^b LCMV gp33 and K^b OVA tetramer binding CD8$^+$ T cells. (G) Number of D^b LCMV gp33, K^b OVA, and L^d QL9 tetramer binding cells per million CD8$^+$ T cells. Each point depicts an individual mouse. Summary data depicts pooled results from (B) 3 independent experiments (n=6/group), (D-E) 2 independent experiments (n=9/group) and (G) 2 independent experiments (n=7-14/group). Statistical analyses performed using (D) Student's unpaired t-test (2-tailed), (G) 1-way ANOVA with Dunnett's multiple comparisons test. Error bars depict SEM. ****$p<0.0001$.

Figure 2. H-L^d QL9$^+$ CD8$^+$ T cells proliferate in the spleen and draining lymph nodes after grafting. (A) C57Bl/6 mice were grafted with H-2^d Balb/c skin. (B) Representative flow cytometry plots and (C) absolute numbers of CD8$^+$ T cells on day 0 or day 10 after grafting in the draining lymph nodes and spleen. (D) Fold change of the number of L^d QL9$^+$ CD8$^+$ T cells on day 10 post-graft relative to day 0 in the draining lymph nodes or spleen. (E) Representative flow cytometry plots and summary data of Ki67 staining among CD44^{hi} L^d QL9$^+$ CD8$^+$ T cell populations in the

draining lymph nodes and spleen. Each data point depicts an individual mouse. Summary data depicts pooled data from (C-D) 4 independent experiments (n=12-17/group) or (E) 2-3 independent experiments (6-9/group). Statistical analyses performed using (C) unpaired Student's t-test (2-tailed), (D) one-way ANOVA with Dunnett's multiple comparisons test. Error bars depict SEM. *p<0.05, **p<0.01, ***p<0.001, ****p<0.0001.

Figure 3. Graft-specific CD8$^+$ T cells maintain clonal diversity throughout the primary effector response. (A) C57Bl/6 mice were grafted with Balb/c skin grafts and multiple tissues were collected. Splenic CD8$^+$ T cell populations were flow cytometrically sorted based on L^d QL9 binding and CD44 expression. (B) Inverse Simpson Index for naïve CD44^{lo} and day 10 effector CD44^{hi} T cell populations are depicted. (C) Frequency of meta-clonotypes in each sample that are defined as hyperexpanded (>1%), large (0.1-1%), medium (0.01-0.1%), small (<0.01%), or are not present. (D) Frequency of meta-clonotypes defined as in (C), found in the skin graft tissue on day 10. (D) CDR3 sequences from 13 convergent meta-clonotypes. Left TCR logo is scaled by per-column relative entropy to background population. The right TCR logo depicts the full meta-clonotype CDR3 sequence. (E) Frequency of meta-clonotypes present in the splenic CD44^{lo} and CD44^{hi} L^d QL9$^+$ populations. (F-G) Number of meta-clonotypes present in peripheral blood mononuclear cells (PBMC) and graft tissue at the depicted timepoints. Each data point depicts an individual mouse. Statistical analysis performed using unpaired Student's t-test. Error bars depict SEM. ***p<0.001, ****p<0.0001.

Figure 4. Post-graft effector CD8$^+$ T cells express activation markers but poorly express KLRG-1. C57Bl/6 mice were grafted with H-2^d Balb/c skin. (A) Representative flow cytometry plots and summary data depicting the frequency of CXCR3$^+$ and CD62L^{lo}CXCR3$^+$ T_{EFF} among (B) bulk CD8$^+$ T cells and (C) L^d QL9$^+$ CD8$^+$ T cells at the indicated timepoints post-graft. (D) Representative flow cytometry plots and (E) summary data depicting the frequency of

CD127^{lo}KLRG1^{+} cells among bulk CD8^{+} T cells and L^{d} QL9^{+} T cells at the indicated timepoints in the spleen. (F) Representative flow cytometry plots and (G) summary data depicting the frequency of CD127^{lo}KLRG-1^{+} cells among bulk CD8^{+} T cells and L^{d} QL9^{+} CD8^{+} T cells at day 0 or day 10 in the graft draining lymph nodes. Each data point depicts an individual mouse. Summary data depicts pooled results from 2-3 independent experiments (n=6-12 mice/group). Error bars depict SEM.

Figure 5. CD8^{+} T cells differentiate into CD43^{+} T effector populations that peak early after grafting. C57Bl/6 mice were grafted with H-2^{d} Balb/c skin and the frequency of L^{d} QL9^{+} and bulk CD8^{+} T cells were assessed in the spleen at the indicated timepoints. (A) UMAP of costimulation and activation markers from day 0, 10, 21, and 42 post-graft CD8^{+} T cell populations. (B) Box plots of the frequency of clusters elevated at day 10 or day 21/42. (C) UMAP depicting day 10 and day 21/42 enriched clusters. (D) Histograms depicting expression of individual markers in day 10 and day 21/42 enriched clusters. (E) Expression of CD43 and CD62L on CD8^{+} T cell populations at day 0, 10, 21, and 42 post-graft. Each data point depicts an individual mouse. Summary data depicts pooled results from (A-D) one (n=4 mice/group), (E) 2-3 independent experiments (n=5-10 mice/group). Statistics performed by (B-C, E) 1-way ANOVA with Dunnett's multiple comparison's test or (G) unpaired Student's t-test. Error bars depict SEM. *$p<0.05$, **$p<0.01$, ***$p<0.001$, ****$p<0.0001$.

Figure 6. CD43^{+} T$_{EFF}$ display potent effector function and mediate graft rejection. (A) C57Bl/6 mice were grafted with H-2^{d} Balb/c skin and L^{d} QL9^{+} and bulk CD8^{+} T cells were assessed in the spleen at day 10-14 post-graft. Representative flow cytometry plots and summary data of (B) Granzyme B^{+} cells and (C) T-BET^{+} cells in the indicated CD8^{+} T$_{EFF}$ populations. (D) Post-graft effectors were stimulated *in vitro* for 5 hours with Balb/c splenocytes and the frequency of IFN-γ

and TNF-α producing cells was assessed. (E) CD45.1$^+$ CD8$^+$ T cells were sorted into CD62L^{lo} CD43$^+$ and CD43$^-$ populations, and 9x10^4 cells/mouse were transferred into congenic hosts that were grafted with Balb/c skin grafts and assessed for survival. (F) Graft survival analysis of C57Bl/6 hosts transferred with CD45.1$^+$ CD8$^+$ T cell populations described in (E). (G) OT-I CD8$^+$ T cells were labeled with CellTrace Violet and stimulated *in vitro* for 3 days in the presence of 0 μM (unstimulated) or 1 μM OVA peptide and the indicated cytokine. (H) Histograms depicting the expression of CD43 and Nur77 on undivided unstimulated or 1 μM peptide divided populations. For each individual experiment, the MFI was normalized to the maximum value of CD43 or Nur77. Each data point depicts an individual mouse. Summary data depicts pooled results from (B-D) 2 independent experiments (n=5-8 mice/group), (F) 2 independent experiments (n=7-15/group), (H) 3 independent experiments with an individual mouse. Statistical analyses performed by (B-D) 1-way ANOVA with Tukey's multiple comparisons test, (F) Log-rank (Mantel-Cox) test, (H) 2-way ANOVA with Dunnett's multiple comparisons test. Error bars depict SEM. *p<0.05, **p<0.01, ****p<0.0001.

Figure 7. ICOS expression is induced on CD43+ T_{EFF} and ICOS blockade prolongs graft survival. (A) Experimental schematic depicting the treatment of C57Bl/6 mice grafted with H-2^d Balb/c skin and treated with CTLA-4 Ig. (B) UMAP expression analysis of day 10 post-graft L^d QL9$^+$ and bulk CD8$^+$ T cells in the spleen in mice untreated or treated with CTLA-4 Ig. (C) UMAP depicting four CD44^{hi} clusters. (D) Histograms of proteins used in UMAP analysis for four CD44^{hi} clusters and the average of all samples. (E) Representative flow cytometry plots and summary data depicting the frequency of CD62L and CD43-expressing effector populations in the spleen on day 10 post-graft in mice. (F) Expression of ICOS on CD8$^+$ T_{EFF} populations in CTLA-4 Ig and control mice. (G) Graft survival of C57Bl/6 mice treated with CTLA-4 Ig or CTLA-4 Ig with anti-ICOS and grafted with a Balb/c skin graft. Each data point depicts an individual mouse. Summary

data depicts pooled results from (E-F) 2 independent experiments (n=6-7 mice/group), (G) 3 independent experiments (n=12-16/group). Statistical analyses performed by (E-F) 2-way ANOVA with Tukey's multiple comparisons test, (G) Log-rank (Mantel-Cox) test. Error bars depict SEM. **$p<0.01$

REFERENCES

Adom, D., Dillon, S.R., Yang, J., Liu, H., Ramadan, A., Kushekhar, K., Hund, S., Albright, A., Kirksey, M., Adeniyan, T., et al. (2020). ICOSL $^{+}$ plasmacytoid dendritic cells as inducer of graft-versus-host disease, responsive to a dual ICOS/CD28 antagonist. Science Translational Medicine *12*. https://doi.org/10.1126/scitranslmed.aay4799.

Amir, A.L., D'Orsogna, L.J.A., Roelen, D.L., van Loenen, M.M., Hagedoorn, R.S., de Boer, R., van der Hoorn, M.A.W.G., Kester, M.G.D., Doxiadis, I.I.N., Falkenburg, J.H.F., et al. (2010). Allo-HLA reactivity of virus-specific memory T cells is common. Blood *115*, 3146–3157. https://doi.org/10.1182/blood-2009-07-234906.

Bozeman, A.M., Laurie, S.J., Haridas, D., Wagener, M.E., and Ford, M.L. (2018). Transplantation preferentially induces a KLRG-1lo CD127hi differentiation program in antigen-specific CD8+ T cells. Transplant Immunology *50*. https://doi.org/10.1016/j.trim.2018.06.003.

Braza, F., Brouard, S., Chadban, S., and Goldstein, D.R. (2016). Role of TLRs and DAMPs in allograft inflammation and transplant outcomes. Nature Reviews Nephrology *12*, 281–290. https://doi.org/10.1038/nrneph.2016.41.

Burrack, A.L., Malhotra, D., Dileepan, T., Osum, K.C., Swanson, L.A., Fife, B.T., and Jenkins, M.K. (2018). Cutting Edge: Allograft Rejection Is Associated with Weak T Cell Responses to Many Different Graft Leukocyte-Derived Peptides. The Journal of Immunology *200*, 477–482. https://doi.org/10.4049/jimmunol.1701434.

Callemeyn, J., Lamarthée, B., Koenig, A., Koshy, P., Thaunat, O., and Naesens, M. (2021). Allorecognition and the spectrum of kidney transplant rejection. Kidney International https://doi.org/10.1016/j.kint.2021.11.029.

Cannon, J.L., Mody, P.D., Blaine, K.M., Chen, E.J., Nelson, A.D., Sayles, L.J., Moore, T. v., Clay, B.S., Dulin, N.O., Shilling, R.A., et al. (2011). CD43 interaction with ezrin-radixin-

moesin (ERM) proteins regulates T-cell trafficking and CD43 phosphorylation. Molecular Biology of the Cell *22*, 954–963. https://doi.org/10.1091/mbc.e10-07-0586.

Chen, J., Eisen, H.N., and Kranz, D.M. (2003). A model T-cell receptor system for studying memory T-cell development. Microbes and Infection *5*, 233–240. https://doi.org/10.1016/S1286-4579(03)00016-9.

Cherukuri, A., Salama, A.D., Mehta, R., Mohib, K., Zheng, L., Magee, C., Harber, M., Stauss, H., Baker, R.J., Tevar, A., et al. (2021). Transitional B cell cytokines predict renal allograft outcomes. Science Translational Medicine *13*. https://doi.org/10.1126/scitranslmed.abe4929.

Chung, H.K., McDonald, B., and Kaech, S.M. (2021). The architectural design of CD8+ T cell responses in acute and chronic infection: Parallel structures with divergent fates. Journal of Experimental Medicine *218*. https://doi.org/10.1084/jem.20201730.

Clark, M.C., and Baum, L.G. (2012). T cells modulate glycans on CD43 and CD45 during development and activation, signal regulation, and survival. Ann N Y Acad Sci *1253*, 58–67. https://doi.org/10.1111/j.1749-6632.2011.06304.x.

Cole, E.H., Johnston, O., Rose, C.L., and Gill, J.S. (2008). Impact of Acute Rejection and New-Onset Diabetes on Long-Term Transplant Graft and Patient Survival. Clinical Journal of the American Society of Nephrology *3*. https://doi.org/10.2215/CJN.04681107.

Colvin, M.M., Smith, C.A., Tullius, S.G., and Goldstein, D.R. (2017). Aging and the immune response to organ transplantation. Journal of Clinical Investigation *127*, 2523–2529. https://doi.org/10.1172/JCI90601.

Crepeau, R.L., and Ford, M.L. (2017). Challenges and opportunities in targeting the CD28/CTLA-4 pathway in transplantation and autoimmunity. Expert Opinion on Biological Therapy *17*, 1001–1012. https://doi.org/10.1080/14712598.2017.1333595.

Dash, P., Fiore-Gartland, A.J., Hertz, T., Wang, G.C., Sharma, S., Souquette, A., Crawford, J.C., Clemens, E.B., Nguyen, T.H.O., Kedzierska, K., et al. (2017). Quantifiable predictive

features define epitope-specific T cell receptor repertoires. Nature *547*, 89–93. https://doi.org/10.1038/nature22383.

Dwyer, G.K., and Turnquist, H.R. (2021). Untangling Local Pro-Inflammatory, Reparative, and Regulatory Damage-Associated Molecular-Patterns (DAMPs) Pathways to Improve Transplant Outcomes. Frontiers in Immunology *12*. https://doi.org/10.3389/fimmu.2021.611910.

Fay, K.T., Chihade, D.B., Chen, C.-W., Klingensmith, N.J., Lyons, J.D., Ramonell, K., Liang, Z., Coopersmith, C.M., and Ford, M.L. (2018). Increased mortality in CD43-deficient mice during sepsis. PLOS ONE *13*, e0202656. https://doi.org/10.1371/journal.pone.0202656.

Felix, N.J., Donermeyer, D.L., Horvath, S., Walters, J.J., Gross, M.L., Suri, A., and Allen, P.M. (2007). Alloreactive T cells respond specifically to multiple distinct peptide-MHC complexes. Nature Immunology *8*, 388–397. https://doi.org/10.1038/ni1446.

Ford, M.L. (2016). T Cell Cosignaling Molecules in Transplantation. Immunity *44*. https://doi.org/10.1016/j.immuni.2016.04.012.

Ford, M.L., and Evavold, B.D. (2006). Modulation of MOG 37–50-specific CD8+ T cell activation and expansion by CD43. Cellular Immunology *240*, 53–61. https://doi.org/10.1016/j.cellimm.2006.06.007.

Ford, M.L., Onami, T.M., Sperling, A.I., Ahmed, R., and Evavold, B.D. (2003). CD43 Modulates Severity and Onset of Experimental Autoimmune Encephalomyelitis. The Journal of Immunology *171*, 6527–6533. https://doi.org/10.4049/jimmunol.171.12.6527.

Ford, M.L., Koehn, B.H., Wagener, M.E., Jiang, W., Gangappa, S., Pearson, T.C., and Larsen, C.P. (2007). Antigen-specific precursor frequency impacts T cell proliferation, differentiation, and requirement for costimulation. Journal of Experimental Medicine *204*, 299–309. https://doi.org/10.1084/jem.20062319.

Haluszczak, C., Akue, A.D., Hamilton, S.E., Johnson, L.D.S., Pujanauski, L., Teodorovic, L., Jameson, S.C., and Kedl, R.M. (2009). The antigen-specific CD8+ T cell repertoire in

unimmunized mice includes memory phenotype cells bearing markers of homeostatic expansion. Journal of Experimental Medicine *206*, 435–448. https://doi.org/10.1084/jem.20081829.

Harper, S.J.F., Ali, J.M., Wlodek, E., Negus, M.C., Harper, I.G., Chhabra, M., Qureshi, M.S., Mallik, M., Bolton, E., Bradley, J.A., et al. (2015). CD8 T-cell recognition of acquired alloantigen promotes acute allograft rejection. Proceedings of the National Academy of Sciences *112*, 12788–12793. https://doi.org/10.1073/pnas.1513533112.

Heeger, P.S., Greenspan, N.S., Kuhlenschmidt, S., Dejelo, C., Hricik, D.E., Schulak, J.A., and Tary-Lehmann, M. (1999). Pretransplant frequency of donor-specific, IFN-gamma-producing lymphocytes is a manifestation of immunologic memory and correlates with the risk of posttransplant rejection episodes. J Immunol *163*, 2267–2275. .

Herndler-Brandstetter, D., Ishigame, H., Shinnakasu, R., Plajer, V., Stecher, C., Zhao, J., Lietzenmayer, M., Kroehling, L., Takumi, A., Kometani, K., et al. (2018a). KLRG1+ Effector CD8+ T Cells Lose KLRG1, Differentiate into All Memory T Cell Lineages, and Convey Enhanced Protective Immunity. Immunity *48*, 716-729.e8. https://doi.org/10.1016/j.immuni.2018.03.015.

Herndler-Brandstetter, D., Ishigame, H., Shinnakasu, R., Plajer, V., Stecher, C., Zhao, J., Lietzenmayer, M., Kroehling, L., Takumi, A., Kometani, K., et al. (2018b). KLRG1+ Effector CD8+ T Cells Lose KLRG1, Differentiate into All Memory T Cell Lineages, and Convey Enhanced Protective Immunity. Immunity *48*, 716-729.e8. https://doi.org/10.1016/j.immuni.2018.03.015.

Jameson, S.C., and Masopust, D. (2018). Understanding Subset Diversity in T Cell Memory. Immunity *48*, 214–226. https://doi.org/10.1016/j.immuni.2018.02.010.

Jenkins, M.K., and Moon, J.J. (2012). The Role of Naive T Cell Precursor Frequency and Recruitment in Dictating Immune Response Magnitude. The Journal of Immunology *188*, 4135–4140. https://doi.org/10.4049/jimmunol.1102661.

Joshi, N.S., Cui, W., Chandele, A., Lee, H.K., Urso, D.R., Hagman, J., Gapin, L., and Kaech, S.M. (2007). Inflammation Directs Memory Precursor and Short-Lived Effector CD8+ T Cell Fates via the Graded Expression of T-bet Transcription Factor. Immunity *27*. https://doi.org/10.1016/j.immuni.2007.07.010.

Kotturi, M.F., Scott, I., Wolfe, T., Peters, B., Sidney, J., Cheroutre, H., von Herrath, M.G., Buchmeier, M.J., Grey, H., and Sette, A. (2008). Naive Precursor Frequencies and MHC Binding Rather Than the Degree of Epitope Diversity Shape CD8 $^{+}$ T Cell Immunodominance. The Journal of Immunology *181*, 2124–2133. https://doi.org/10.4049/jimmunol.181.3.2124.

Krummey, S.M., Martinez, R.J., Andargachew, R., Liu, D., Wagener, M., Kohlmeier, J.E., Evavold, B.D., Larsen, C.P., and Ford, M.L. (2016). Low-Affinity Memory CD8 $^{+}$ T Cells Mediate Robust Heterologous Immunity. The Journal of Immunology *196*, 2838–2846. https://doi.org/10.4049/jimmunol.1500639.

Liu, D., Krummey, S.M., Badell, I.R., Wagener, M., Schneeweis, L.A., Stetsko, D.K., Suchard, S.J., Nadler, S.G., and Ford, M.L. (2014). 2B4 (CD244) induced by selective CD28 blockade functionally regulates allograft-specific CD8+ T cell responses. Journal of Experimental Medicine *211*, 297–311. https://doi.org/10.1084/jem.20130902.

Macedo, C., Orkis, E.A., Popescu, I., Elinoff, B.D., Zeevi, A., Shapiro, R., Lakkis, F.G., and Metes, D. (2009). Contribution of Naïve and Memory T-Cell Populations to the Human Alloimmune Response. American Journal of Transplantation *9*, 2057–2066. https://doi.org/10.1111/j.1600-6143.2009.02742.x.

Meier-Kriesche, H.-U., Ojo, A.O., Hanson, J.A., Cibrik, D.M., Punch, J.D., Leichtman, A.B., and Kaplan, B. (2000). Increased Impact of Acute Rejection on Chronic Allograft Failure in Recent Era. Transplantation *70*. https://doi.org/10.1097/00007890-200010150-00018.

Milner, J.J., Nguyen, H., Omilusik, K., Reina-Campos, M., Tsai, M., Toma, C., Delpoux, A., Boland, B.S., Hedrick, S.M., Chang, J.T., et al. (2020). Delineation of a molecularly distinct

terminally differentiated memory CD8 T cell population. Proceedings of the National Academy of Sciences *117*, 25667–25678. https://doi.org/10.1073/pnas.2008571117.

Mody, P.D., Cannon, J.L., Bandukwala, H.S., Blaine, K.M., Schilling, A.B., Swier, K., and Sperling, A.I. (2007). Signaling through CD43 regulates CD4 T-cell trafficking. Blood *110*, 2974–2982. https://doi.org/10.1182/blood-2007-01-065276.

Moon, J.J., Chu, H.H., Pepper, M., McSorley, S.J., Jameson, S.C., Kedl, R.M., and Jenkins, M.K. (2007). Naive CD4+ T Cell Frequency Varies for Different Epitopes and Predicts Repertoire Diversity and Response Magnitude. Immunity *27*, 203–213. https://doi.org/10.1016/j.immuni.2007.07.007.

Moon, J.J., Chu, H.H., Hataye, J., Pagán, A.J., Pepper, M., McLachlan, J.B., Zell, T., and Jenkins, M.K. (2009). Tracking epitope-specific T cells. Nature Protocols *4*, 565–581. https://doi.org/10.1038/nprot.2009.9.

Moran, A.E., Holzapfel, K.L., Xing, Y., Cunningham, N.R., Maltzman, J.S., Punt, J., and Hogquist, K.A. (2011). T cell receptor signal strength in Treg and iNKT cell development demonstrated by a novel fluorescent reporter mouse. Journal of Experimental Medicine *208*, 1279–1289. https://doi.org/10.1084/jem.20110308.

Nolz, J.C., and Harty, J.T. (2014). IL-15 regulates memory CD8+ T cell O-glycan synthesis and affects trafficking. Journal of Clinical Investigation *124*, 1013–1026. https://doi.org/10.1172/JCI72039.

Obar, J.J., Khanna, K.M., and Lefrançois, L. (2008). Endogenous Naive CD8+ T Cell Precursor Frequency Regulates Primary and Memory Responses to Infection. Immunity *28*, 859–869. https://doi.org/10.1016/j.immuni.2008.04.010.

Onami, T.M., Harrington, L.E., Williams, M.A., Galvan, M., Larsen, C.P., Pearson, T.C., Manjunath, N., Baum, L.G., Pearce, B.D., and Ahmed, R. (2002). Dynamic Regulation of T Cell Immunity by CD43. The Journal of Immunology *168*, 6022–6031. https://doi.org/10.4049/jimmunol.168.12.6022.

Peng, C., Huggins, M.A., Wanhainen, K.M., Knutson, T.P., Lu, H., Georgiev, H., Mittelsteadt, K.L., Jarjour, N.N., Wang, H., Hogquist, K.A., et al. (2022). Engagement of the costimulatory molecule ICOS in tissues promotes establishment of CD8+ tissue-resident memory T cells. Immunity *55*, 98-114.e5. https://doi.org/10.1016/j.immuni.2021.11.017.

Richer, M.J., Pewe, L.L., Hancox, L.S., Hartwig, S.M., Varga, S.M., and Harty, J.T. (2015). Inflammatory IL-15 is required for optimal memory T cell responses. Journal of Clinical Investigation *125*, 3477–3490. https://doi.org/10.1172/JCI81261.

Sarkar, S., Kalia, V., Haining, W.N., Konieczny, B.T., Subramaniam, S., and Ahmed, R. (2008). Functional and genomic profiling of effector CD8 T cell subsets with distinct memory fates. Journal of Experimental Medicine *205*, 625–640. https://doi.org/10.1084/jem.20071641.

Siu, J.H.Y., Surendrakumar, V., Richards, J.A., and Pettigrew, G.J. (2018). T cell Allorecognition Pathways in Solid Organ Transplantation. Frontiers in Immunology *9*. https://doi.org/10.3389/fimmu.2018.02548.

Solinas, C., Gu-Trantien, C., and Willard-Gallo, K. (2020). The rationale behind targeting the ICOS-ICOS ligand costimulatory pathway in cancer immunotherapy. ESMO Open *5*. https://doi.org/10.1136/esmoopen-2019-000544.

Sperling, A.I., Green, J.M., Mosley, R.L., Smith, P.L., DiPaolo, R.J., Klein, J.R., Bluestone, J.A., and Thompson, C.B. (1995). CD43 is a murine T cell costimulatory receptor that functions independently of CD28. Journal of Experimental Medicine *182*, 139–146. https://doi.org/10.1084/jem.182.1.139.

Suchin, E.J., Langmuir, P.B., Palmer, E., Sayegh, M.H., Wells, A.D., and Turka, L.A. (2001). Quantifying the Frequency of Alloreactive T Cells In Vivo: New Answers to an Old Question. The Journal of Immunology *166*, 973–981. https://doi.org/10.4049/jimmunol.166.2.973.

Sykulev, Y., Brunmark, A., Tsomides, T.J., Kageyama, S., Jackson, M., Peterson, P.A., and Eisen, H.N. (1994a). High-affinity reactions between antigen-specific T-cell receptors and peptides associated with allogeneic and syngeneic major histocompatibility complex class I

proteins. Proceedings of the National Academy of Sciences *91*, 11487–11491. https://doi.org/10.1073/pnas.91.24.11487.

Sykulev, Y., Brunmark, A., Jackson, M., Cohen, R.J., Peterson, P.A., and Eisen, H.N. (1994b). Kinetics and affinity of reactions between an antigen-specific T cell receptor and peptide-MHC complexes. Immunity *1*, 15–22. https://doi.org/10.1016/1074-7613(94)90005-1.

Sykulev, Y., Joo, M., Vturina, I., Tsomides, T.J., and Eisen, H.N. (1996). Evidence that a Single Peptide–MHC Complex on a Target Cell Can Elicit a Cytolytic T Cell Response. Immunity *4*, 565–571. https://doi.org/10.1016/S1074-7613(00)80483-5.

Trambley, J., Bingaman, A.W., Lin, A., Elwood, E.T., Waitze, S.-Y., Ha, J., Durham, M.M., Corbascio, M., Cowan, S.R., Pearson, T.C., et al. (1999). Asialo GM1+ CD8+ T cells play a critical role in costimulation blockade–resistant allograft rejection. Journal of Clinical Investigation *104*, 1715–1722. https://doi.org/10.1172/JCI8082.

Udaka, K., Tsomides, T.J., and Eisen, H.N. (1992). A naturally occurring peptide recognized by alloreactive CD8+ cytotoxic T lymphocytes in association with a class I MHC protein. Cell *69*, 989–998. https://doi.org/10.1016/0092-8674(92)90617-L.

Udaka, K., Wiesmüller, K.H., Kienle, S., Jung, G., and Walden, P. (1996). Self-MHC-restricted peptides recognized by an alloreactive T lymphocyte clone. J Immunol *157*, 670–678. .

Young, J.S., McIntosh, C., Alegre, M.-L., and Chong, A.S. (2017). Evolving Approaches in the Identification of Allograft-Reactive T and B Cells in Mice and Humans. Transplantation *101*, 2671–2681. https://doi.org/10.1097/TP.0000000000001847.

METHODS

Mice. C57BL/6J and C57BL/6J Ly5.2-Cr (CD45.1) strains were obtained from The Jackson Laboratory (Bar Harbor, Maine) at 6-8 weeks of age. Balb/cJ, C57Bl/6-Tg(TcraTcrb)1100Mjb/J (OT-I), and RAG1^{tm1Mom} (RAG1 knockout) were obtained from The Jackson Laboratory and bred at Emory University or Johns Hopkins University. All transplant experiments were conducted in age-matched hosts randomly assigned to experimental groups. This study was conducted in accordance with the recommendations in the Guide for the Care and Use of Laboratory Animals. The protocol was approved by the Animal Care and Use Committee at Emory University and Johns Hopkins University. Animals were housed in specific pathogen-free animal facilities at Emory University and Johns Hopkins University.

Skin Grafting. Full-thickness tail and ear skins were transplanted onto the dorsal thorax of recipient mice and secured with adhesive bandages as previously described (Trambley et al., 1999). In some experiments, mice were treated with 250 ug/dose of CTLA-4 Ig (BioXCell) and anti-ICOS (BioXCell) via i.p. injection on day 0, 2, 4, and 6.

MHC Tetramers and CD8$^+$ T cell Enrichment. MHC tetramers with human β2-microglobulin specific for QL9 (H-2L^d QLSPFPFDL), LCMV gp33 (H-2D^b KAVYFATC), and OVA (H-2K^b SIINFEKL) were obtained from the NIH Tetramer Core facility. Tetramer enrichment was performed based on published protocols (Moon et al., 2009). Briefly, single cell suspensions of splenocytes or lymphocytes were incubated with MHC tetramer (PE or APC), followed by incubation with anti-PE or anti-APC paramagnetic microbeads (Miltenyi), and enrichment over an LS column (Miltenyi). The column flow through was collected as the unbound fraction containing bulk CD8$^+$ T cells and the column bound fraction enriched for tetramer binding cells were stained

for surface and intracellular antigens and analyzed by flow cytometry. Absolute cell counts were performed using CountBrite beads (BD Biosciences) or Cytek Aurora.

Antibodies and Flow Cytometry. Flow cytometry and magnetic enrichment were performed in 1X PBS (without Ca^{2+}/Mg^{2+}, pH 7.2), 0.25% BSA, 2 mM EDTA, and 0.09% azide. Single cell suspensions were incubated in 96-well U-bottom plates with the following antibodies for 30-60 min at room temperature: CD4, CD8, CD11c, F4/80, CD19, CD27, CD28, CD127, KLRG-1, CD43, CXCR3, CD62L, ICOS, CD44, CD62L. Intracellular staining was performed using the Transcription Factor Staining Kit (eBiosciences) and the following antigens: Ki67, Nur77, Granzyme B, T-Bet, IFN-γ, TNF-α. Dead cells were excluded with Live/Dead Aqua (Invitrogen), Live/Dead Near IR (Biolegend), or propidium iodide (Invitrogen) according to manufacturer's instructions.

***Ex vivo* Allogeneic Stimulation for Cytokine Production**. Splenocytes and draining lymph node cells from $CD45.1^+$ mice grafted with Balb/c skin grafts 14 days prior were processed to single cell suspension and pooled. $1.5x10^6$ CD45.1 cells were incubated with $2x10^6$ Balb/c splenocytes in the presence of 1 mg/mL GolgiStop (Invitrogen) for 4-5 h at 37 C. Cells were collected and gated on $CD45.1^+$ $CD8^+$ T cells for intracellular cytokine analysis.

Flow cytometric cell sorting and adoptive transfer. Splenocytes and draining lymph nodes cells from $CD45.1^+$ mice grafted with Balb/c skin grafts 10-14 days prior were stained to identify effector $CD62L^{lo}CD43^+$ and $CD62L^{lo}CD43^-$ $CD8^+$ T cells. Cells were sorted on a MoFlo XDP. $9x10^4$ purified cells were transferred via tail vein into C57BL/6J mice. Mice were grafted the following day with Balb/c skin and monitored for graft survival.

***In vitro* OT-I Stimulation**. Naïve OT-I splenocytes were stained with CellTrace Violet (Invitrogen) according to the manufacturer's instructions and plated in 24 well tissue culture plates at $3x10^6$/well in in the presence of OT-I peptide (GenScript) and the following cytokines: CpG (3.125 μg/mL, Invivogen), IFN-α (Biolegend, 1.1 μg/mL), IL-12 (Biolegend, 10 ng/mL), IL-15 (Biolegend, 10 ng/mL), IFN-γ (Biolegend, 100 ng/mL). Cells were incubated in Complete R10 media comprised of RPMI 1640 with L-glutamine (Corning), 10% FBS, 100 mM HEPES, 500 uM β-mercaptoethanol, 100 U/mL penicillin/stremptomycin at 37 C (5% CO_2) for 72 h prior to analysis by flow cytometry.

***TCRB* Sequencing (FR3AK-Seq) and Analysis**. $CD8^+$ T cell populations from splenocytes and draining lymph nodes were flow cytometrically sorted from naïve or post-Balb/c skin graft mice as described above. RNA was isolated using the RNEasy Plus Mini kit (Qiagen) according to manufacturer instructions. cDNA was generated using the Superscript IV First-Strand Synthesis System kit per manufacturer protocol instructions. A normalized input of 200ng of RNA was used for each sample, or if the concentration was too low to reach 200ng, the maximum amount of RNA that could be input into the reaction was used. RNA corresponding to 1000 cells of the EL4 cell-line was used as a spike-in in all samples. cDNA samples were cleaned-up and concentrated using the Zymo Research ZR-96 DNA Clean and Concentrator kit (cat# D4023). 20 cycles of PCR1 were performed using the KAPA2G Fast Multiplex Mix and primers designed to encompass all mouse TCRBV alleles. 20 cycles of PCR2 was performed for sample barcoding. Sequencing was performed on an Illumina NextSeq. CDR3s were identified and quantified using MiXCR software (v 3.0.13), and the EL4 spike-in was used to normalize MiXCR clone counts.

Assembled clonotypes were imported and analyzed in R (4.1.1) via the immunarch (0.6.7) package. Clonotypes were categorized for expansion based on the relative frequency it

represented in that sample using raw clone counts as follows: >1% hyper-expanded, 1%-0.1% large, 0.1%-0.01% medium, <0.01% small. Graphics were generated with ggplot2 (3.3.5). For any analysis, that required a defined v or j gene and there was an ambiguous result, the top hit was taken. Metaclonotypes were generated in python (3.8.12) using tcrdist3 (0.2.2). Data were imported using pandas (1.3.4). The enriched clonotypes consisted of sorted spleen cells, that were tetramer bound, and $CD44^{hi}$. The background set was generated from naïve mouse blood samples (n=14). A random sample of 280,000 of these clonotypes were generated with tcrsampler (0.1.9), and a v-j matched background of 280,000 clonotypes was generated with olga (1.2.4).

Flow Cytometry Analysis. In all analysis, $CD8^+$ T cells were identified as singlet events, Live/Dead $stain^-$, dump $gate^-$ (CD11c, F4/80, NK1.1, CD19), $CD4^-$, $CD8^+$ events. Manual gating was performed in Flowjo 10. Tetramer and bulk $CD8^+$ T_{EFF} are defined as $CD44^{hi}CD8^+$ T cells. For dimensionality reduction analysis, manually gated unbound $CD8^+$ T cells and bound fraction L^d $QL9^+$ $CD8^+$ T cells events were imported into R (4.1.1) through CytoML (2.40), flowWorkspace (4.4.0), and flowCore (2.4.0). Markers were transformed by hyperbolic arcsine with a cofactor of either 1000 or 6000 depending on the marker. The data were further analyzed using CATALYST (1.16.2) with FlowSOM (2.0.0) clustering and ConsensusClusterPlus (1.56.0) meta clustering. UMAP dimensionality reductions were generated with scatter (1.20.1). Visualizations were generated in ggplot2 (3.3.5) and ComplexHeatmap (2.8.0).

Statistical Analysis. All data points represent individual mice, and where individual data points are not depicted the value of n is provided in the corresponding figure legend. For analysis of absolute numbers and expression levels, paired or unpaired Student's t-tests (two-tailed) were performed between two groups; one-way or two-way ANOVA with multiple comparison tests were used to compare multiple groups. Log-rank (Mantel-cox) test was used to evaluate graft survival

between groups. In vitro CD43 and Nur77 expression data was normalized to the maximum MFI obtained for each marker in a given experiment. Error bars represent standard error measurements (SEM). Statistics were performed using GraphPad Prism 9. Significance was determined as *$p<0.05$, **$p<0.01$, ***$p<0.001$, ****$p<0.0001$.

1 **SUPPLEMENTAL INFORMATION**

CDR3	*TCRB-V* Gene	*TCRB-J* Gene	PGEN	Radius	Chi^2 Dist	Regex	Chi^2 Regex	Chi^2 Joint	K Neighbors	N Subject
CASSDLGGYAEQFF	TRBV13-1*01	TRBJ2-1*01	1.42E-06	0	883.5	(SDLGGYAEQ)	823.9	1707.4	11	5
CASSDALQLYF	TRBV13-1*01	TRBJ2-2*01	2.20E-09	20	580.2	(SDAL[QE][QLV])	701.1	1281.3	7	3
IAISTGTETLYF	TRBV16*01	TRBJ2-3*01	0	0	191.8	(STGTETL)	1031.4	1223.1	3	3
CASSEGAGQLYF	TRBV13-1*01	TRBJ2-2*01	5.19E-07	8	305.0	(SEGAGQL)	853.1	1158.1	4	4
CASSELGGYAEQFF	TRBV13-1*01	TRBJ2-1*01	1.20E-06	0	521.7	(SELGGYAEQ)	397.6	919.4	7	3
CASSDSNTEVFF	TRBV13-1*01	TRBJ1-1*01	2.43E-06	0	525.3	(SDSNTEV)	373.8	899.1	7	4
CGSTGTETLYF	TRBV15*01	TRBJ2-3*01	1.91E-10	10	231.5	(TGTETL)	569.0	800.5	3	3
CASSSTGPEVFF	TRBV4*01	TRBJ1-1*01	6.47E-08	20	319.5	(S[QFS][T]?GPEV)	436.3	755.8	4	4
CASSLDNYAEQFF	TRBV16*01	TRBJ2-1*01	5.77E-06	0	406.4	(SLDNYAEQ)	330.8	737.2	6	4
CASSGGISYEQYF	TRBV13-1*01	TRBJ2-7*01	4.71E-07	10	319.5	(SGG[IV]SYEQ)	319.2	638.8	4	3
CASSDRVEQYF	TRBV13-1*01	TRBJ2-7*01	1.80E-06	0	434.1	(SDRVEQ)	188.5	622.5	6	4
CASSDGTGNTEVFF	TRBV13-1*01	TRBJ1-1*01	9.46E-07	0	267.3	(SDGTGNTEV)	267.3	534.7	4	3
CASGDGRNTEVFF	TRBV13-2*01	TRBJ1-1*01	7.05E-07	0	260.2	(GDGRNTEV)	260.2	520.5	4	3
CASRDSQNALYF	TRBV13-2*01	TRBJ2-4*01	4.01E-13	20	501.1	(RDSQN[AT]L)	15.1	516.2	6	3
CASGPGGEQYF	TRBV13-2*01	TRBJ2-7*01	1.23E-06	0	294.6	(GPGGEQ)	220.7	515.3	4	3
CASRDSQNTLYF	TRBV13-2*01	TRBJ2-4*01	3.43E-06	10	501.1	(R[ND]SQNTL)	11.1	512.2	6	3
CASSDANTEVFF	TRBV13-1*01	TRBJ1-1*01	2.78E-06	0	311.4	(SDANTEV)	165.4	476.8	5	3
CASSDGGNQAPLF	TRBV13-1*01	TRBJ1-5*01	9.06E-07	8	214.4	(S[DE]GGNQAP)	257.9	472.3	3	3
CASSDAGQITEVFF	TRBV13-1*01	TRBJ1-1*01	4.89E-09	10	231.5	(SDAGQITEV)	231.5	463.0	3	3
CASSLDNYAEQFF	TRBV3*01	TRBJ2-1*01	5.77E-06	0	127.4	(SLDNYAEQ)	330.8	458.2	3	3
CASGEGAEQFF	TRBV13-2*01	TRBJ2-1*01	1.09E-06	0	418.0	(GEGAEQ)	39.5	457.5	6	4
CASSSGGEVFF	TRBV16*01	TRBJ1-1*01	6.46E-07	4	231.5	(SSGGEV)	212.0	443.5	3	3
CASSGLGGYAEQFF	TRBV13-1*01	TRBJ2-1*01	8.18E-06	0	264.7	(SGLGGYAEQ)	169.6	434.3	4	3
CASSGGVEQYF	TRBV13-1*01	TRBJ2-7*01	1.63E-06	8	308.9	(SGGVEQ)	78.7	387.6	4	3
CASRDNTEVFF	TRBV13-2*01	TRBJ1-1*01	1.74E-06	0	357.1	(RDNTEV)	28.9	386.0	5	3
CASSLAEQYF	TRBV12-2*01	TRBJ2-7*01	6.03E-06	0	275.1	(SLAEQ)	105.7	380.9	5	4
CASSENTEVFF	TRBV13-1*01	TRBJ1-1*01	4.12E-06	0	267.3	(SENTEV)	94.7	362.1	4	3
CASSEGGAGNTLYF	TRBV13-1*01	TRBJ1-3*01	5.37E-07	0	176.8	(SEGGAGNTL)	176.8	353.5	3	3
CASSDGGEQYF	TRBV13-1*01	TRBJ2-7*01	4.04E-06	0	231.4	(SDGGEQ)	92.6	324.0	4	3
CASSDFEQYF	TRBV13-1*01	TRBJ2-7*01	3.80E-07	0	191.8	(SDFEQ)	123.9	315.7	3	3
CASRQNTEVFF	TRBV13-2*01	TRBJ1-1*01	5.48E-06	8	302.8	(R[QE]NTEV)	3.4	306.2	4	3
CASSDRDERYF	TRBV29*01	TRBJ2-7*01	7.17E-13	14	231.5	(SDRDE[RQ])	74.3	305.8	3	3
CASSDNNNQAPLF	TRBV13-1*01	TRBJ1-5*01	1.78E-06	0	185.6	(SDNNNQAP)	97.8	283.4	3	3
CASSGGAEQFF	TRBV13-1*01	TRBJ2-1*01	1.60E-05	0	243.6	(SGGAEQ)	32.4	276.1	4	4
CASSDTGYEQYF	TRBV13-1*01	TRBJ2-7*01	1.47E-06	0	158.6	(SDTGYEQ)	99.3	257.9	3	3
CASSRDRANTGQLYF	TRBV17*01	TRBJ2-2*01	4.10E-06	0	177.2	(SRDRANTGQL)	70.7	247.9	3	3
CASRQNYEQYF	TRBV13-2*01	TRBJ2-7*01	3.48E-07	10	231.5	(RQ[NS]YEQ)	16.0	247.5	3	3
CASTGGALEQYF	TRBV13-3*01	TRBJ2-7*01	1.45E-07	8	231.5	(TGGALEQ)	5.9	237.4	3	3
CASSASYEQYF	TRBV13-1*01	TRBJ2-7*01	3.62E-06	0	185.3	(SASYEQ)	36.2	221.6	3	3

CASSDSYEQYF	TRBV13-1*01	TRBJ2-7*01	9.06E-06	0	185.3	(SDSYEQ)	35.9	221.3	3	3
CASSGGGEQYF	TRBV13-1*01	TRBJ2-7*01	1.12E-05	0	158.6	(SGGGEQ)	61.1	219.7	3	3
CASSGGGSYEQYF	TRBV13-1*01	TRBJ2-7*01	5.92E-06	0	185.3	(SGGGSYEQ)	31.0	216.4	3	3
CASSGYEQYF	TRBV13-1*01	TRBJ2-7*01	2.14E-05	0	185.3	(SGYEQ)	7.2	192.6	3	3

Table S1. Meta-clonotypes identified in naïve and effector L^d $QL9^+$ effector $CD8^+$ T cells. *TCRB* CDR3 sequences from sorted L^d QL9+ and bulk T cell populations were analyzed using the tcrDist package. Forty-three meta-clonotypes were identified that met criteria of being enriched over background populations and present in more than two samples.

Figure S1. Bulk $CD8^+$ T cells proliferate in the spleen and draining lymph nodes after grafting. Related to Figure 2. C57Bl/6 mice were grafted with H-2^d Balb/c skin. Representative flow cytometry plots and summary data of Ki67 staining among $CD44^{hi}$ $CD8^+$ T cell populations in the draining lymph nodes and spleen. Each data point depicts an individual mouse. Summary data depicts pooled results from 2-3 independent experiments (6-9/group). Statistical analysis performed using one-way ANOVA with Dunnett's multiple comparisons test. Error bars depict SEM. *p<0.05, **p<0.01, ***p<0.001, ****p<0.0001.

Figure S2. CTLA-4 Ig reduces the frequency of proliferating effector $CD4^+$ T cells but not $CD8^+$ T cells. Related to Figure 7. C57Bl/6 mice were grafted with H-2^d Balb/c skin and treated with CTLA-4 Ig or untreated. On day 14 after grafting, the phenotype of $CD4^+$ and $CD8^+$ T cells was assessed in the spleen. Each data point depicts an individual mouse. Summary data depicts pooled results from 2 independent experiments (9/group). Statistical analysis performed using unpaired Student's t-test. Error bars depict SEM. ****p<0.0001.

Figure 1

A

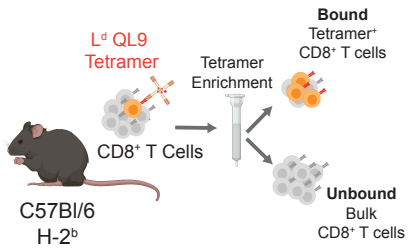

B

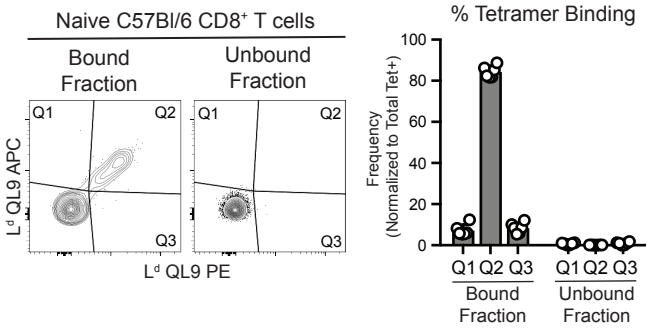

C

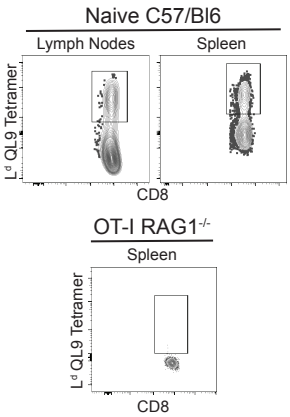

D

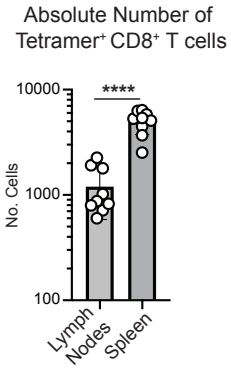

E

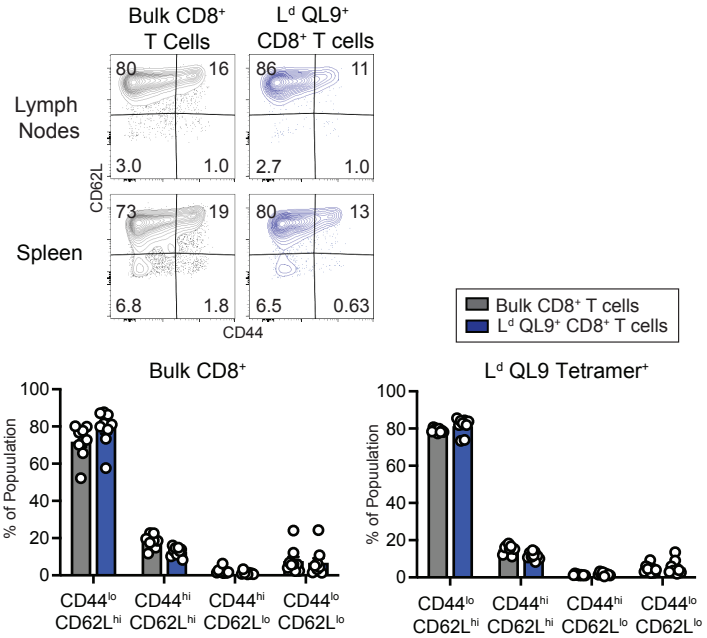

F

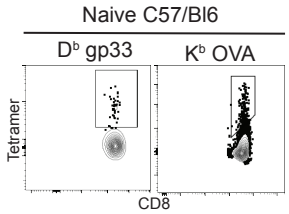

G

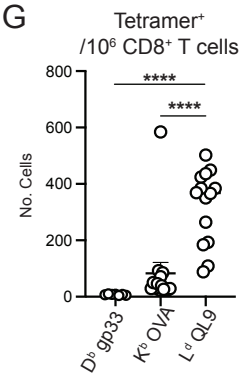

Figure 2

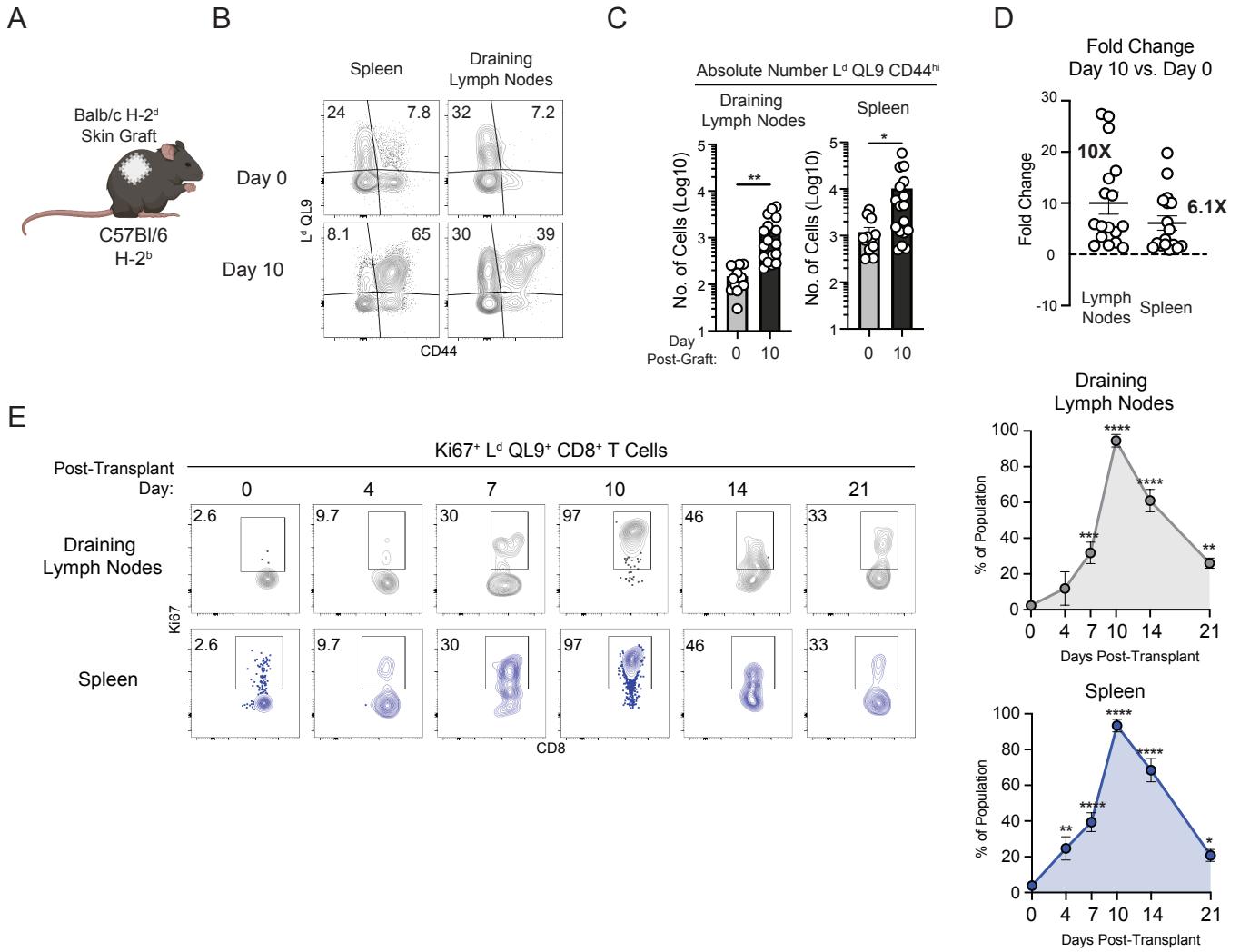
A
Balb/c H-2d
Skin Graft
C57Bl/6
H-2b
B
Spleen
Draining
Lymph Nodes
Day 0
Day 10
Ld QL9
CD44
24
7.8
32
7.2
8.1
65
30
39
C
Absolute Number Ld QL9 CD44hi
Draining
Lymph Nodes
Spleen
No. of Cells (Log10)
Day
Post-Graft:
0
10
D
Fold Change
Day 10 vs. Day 0
Fold Change
10X
6.1X
Lymph
Nodes
Spleen
E
Ki67+ Ld QL9+ CD8+ T Cells
Post-Transplant
Day:
0
4
7
10
14
21
Draining
Lymph Nodes
Spleen
Ki67
CD8
2.6
9.7
30
97
46
33
Draining
Lymph Nodes
Spleen
% of Population
Days Post-Transplant

Figure 3

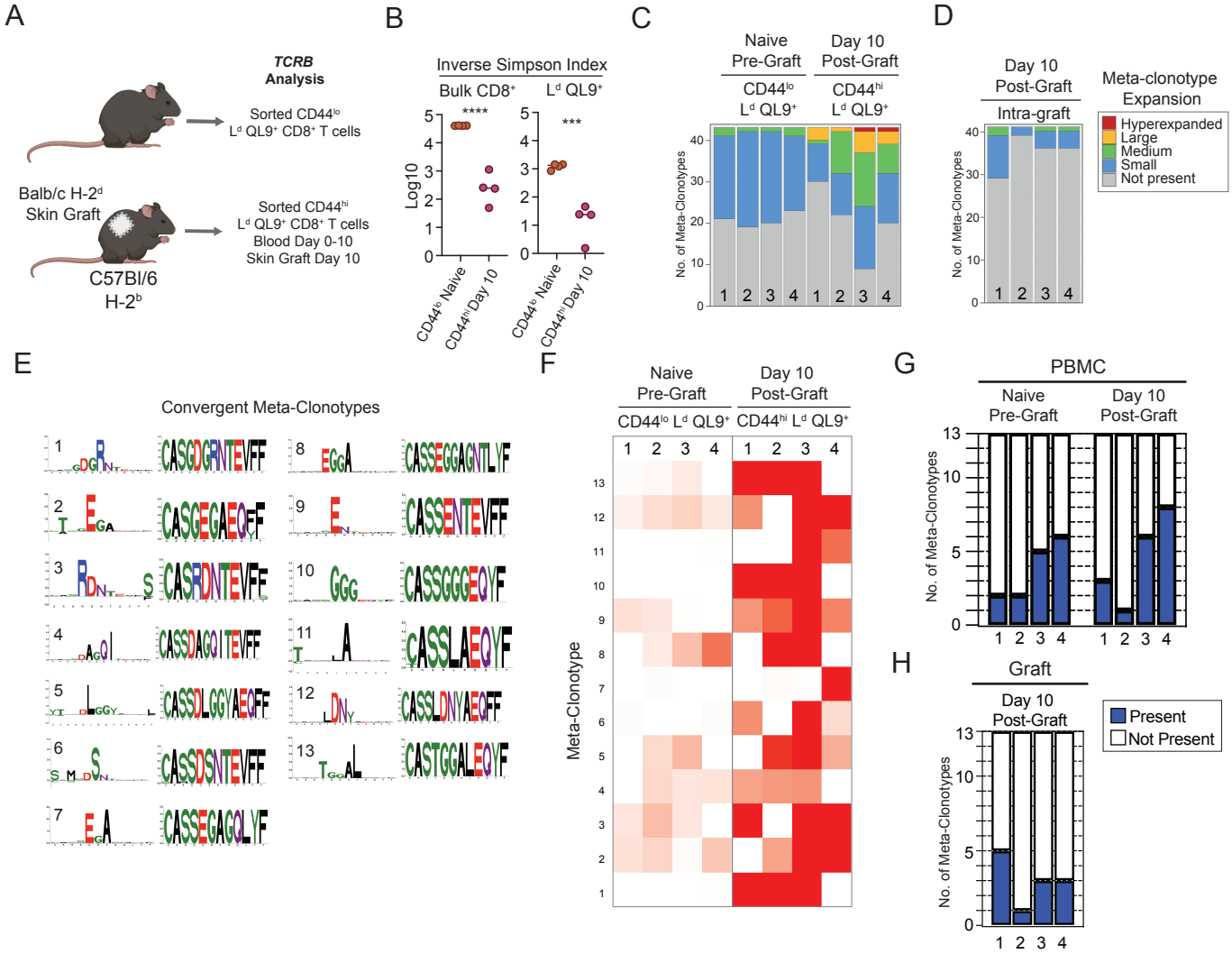
A
TCRB Analysis
Sorted CD44lo Ld QL9+ CD8+ T cells
Balb/c H-2d Skin Graft
Sorted CD44hi Ld QL9+ CD8+ T cells
Blood Day 0-10
Skin Graft Day 10
C57Bl/6 H-2b
B
Inverse Simpson Index
Bulk CD8+
Ld QL9+
Log10
CD44lo Naive
CD44hi Day 10
C
Naive Pre-Graft
Day 10 Post-Graft
CD44lo Ld QL9+
CD44hi Ld QL9+
No. of Meta-Clonotypes
D
Day 10 Post-Graft
Intra-graft
Meta-clonotype Expansion
Hyperexpanded
Large
Medium
Small
Not present
E
Convergent Meta-Clonotypes
F
Meta-Clonotype
G
PBMC
H
Graft
Present
Not Present

Figure 4

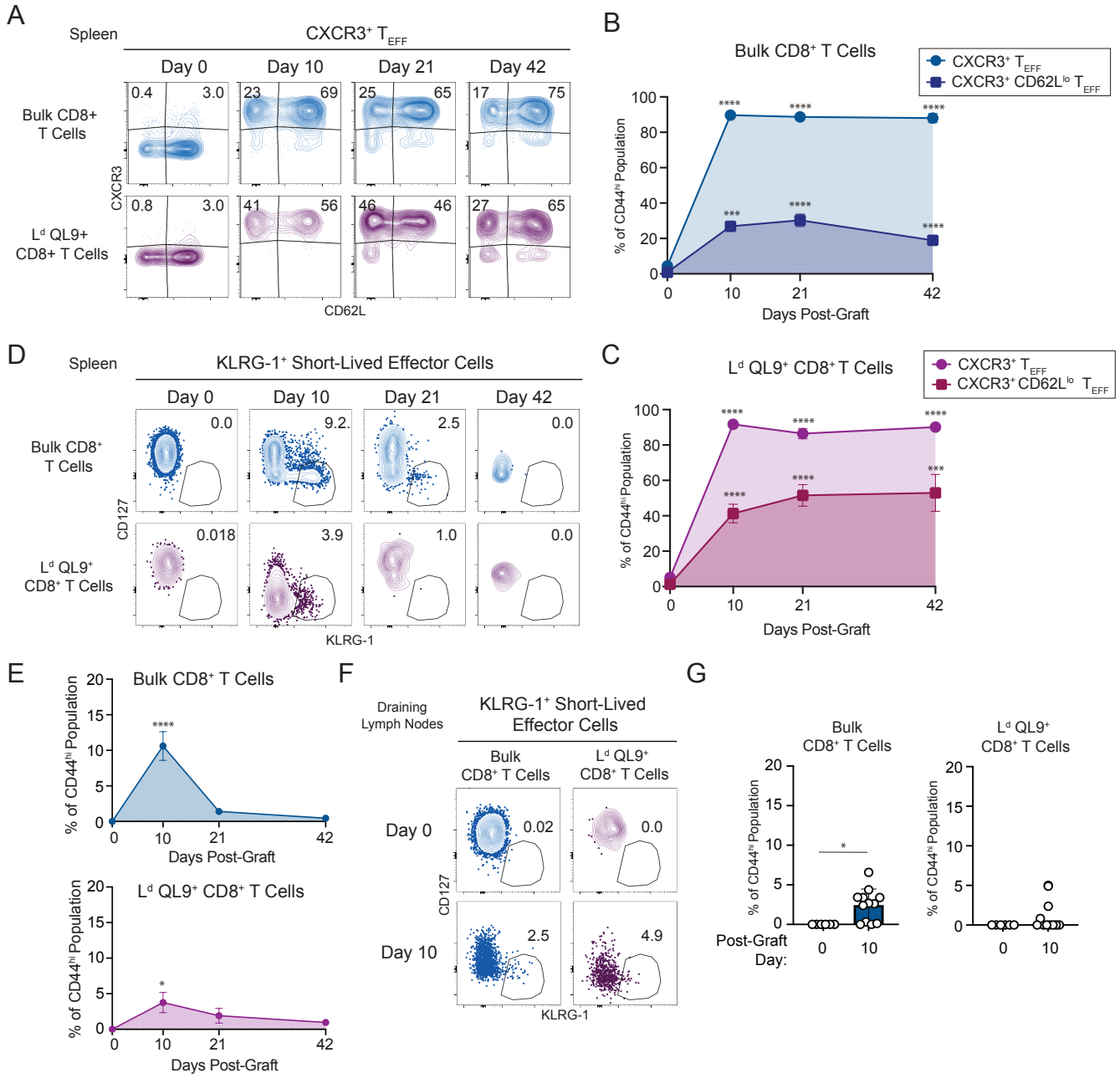
A
Spleen
CXCR3+ TEFF
Day 0
Day 10
Day 21
Day 42
Bulk CD8+ T Cells
Ld QL9+ CD8+ T Cells
CXCR3
CD62L
0.4
3.0
23
69
25
65
17
75
0.8
3.0
41
56
46
46
27
65
B
Bulk CD8+ T Cells
CXCR3+ TEFF
CXCR3+ CD62Llo TEFF
% of CD44hi Population
Days Post-Graft
C
Ld QL9+ CD8+ T Cells
D
Spleen
KLRG-1+ Short-Lived Effector Cells
CD127
KLRG-1
0.0
9.2
2.5
0.0
0.018
3.9
1.0
0.0
E
Bulk CD8+ T Cells
Ld QL9+ CD8+ T Cells
F
Draining Lymph Nodes
KLRG-1+ Short-Lived Effector Cells
Bulk CD8+ T Cells
Ld QL9+ CD8+ T Cells
Day 0
Day 10
0.02
0.0
2.5
4.9
G
Bulk CD8+ T Cells
Ld QL9+ CD8+ T Cells
Post-Graft Day:

Figure 5

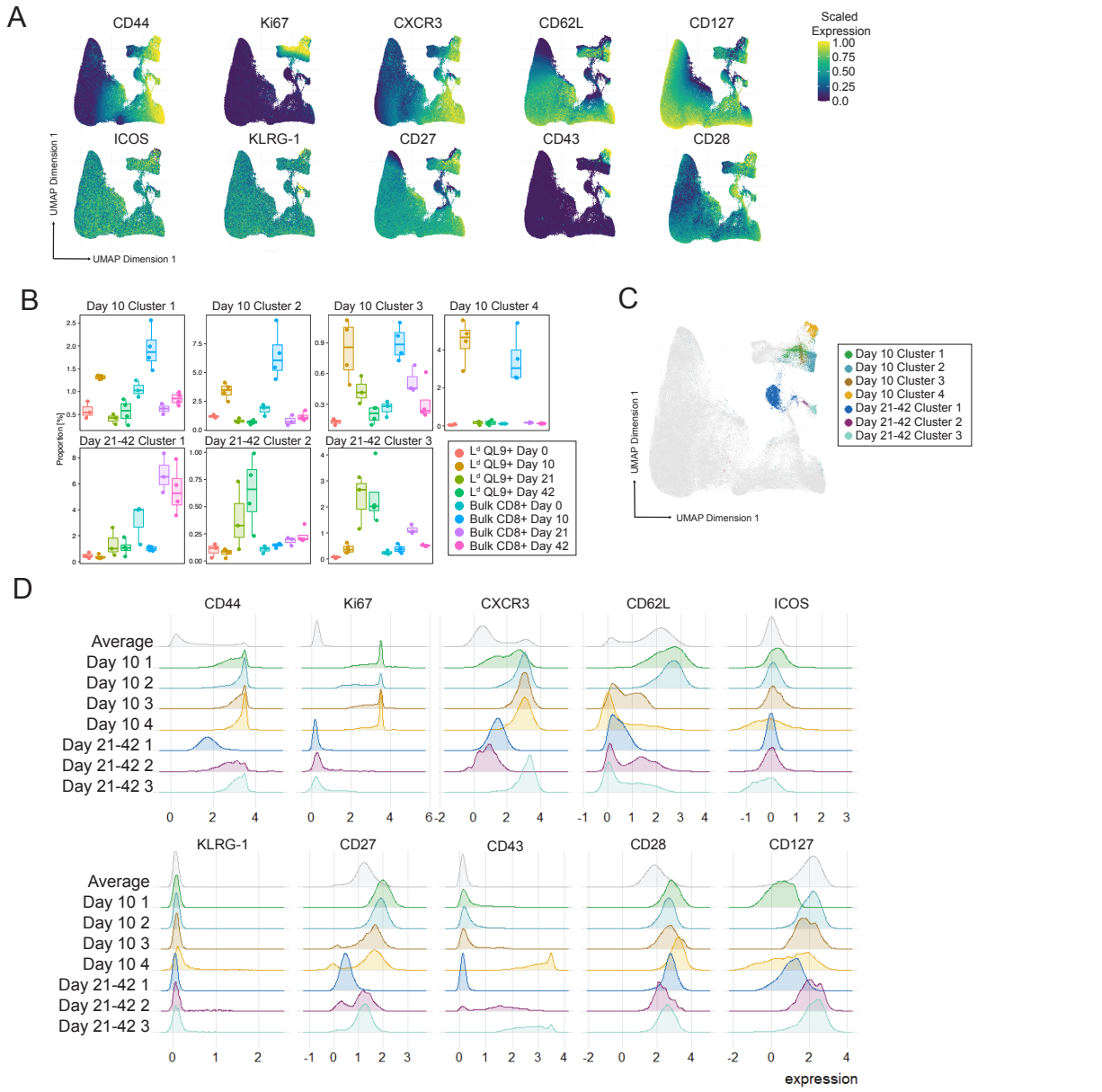
A
CD44
Ki67
CXCR3
CD62L
CD127
ICOS
KLRG-1
CD27
CD43
CD28
Scaled Expression
1.00
0.75
0.50
0.25
0.0
UMAP Dimension 1
UMAP Dimension 1
B
Day 10 Cluster 1
Day 10 Cluster 2
Day 10 Cluster 3
Day 10 Cluster 4
Day 21-42 Cluster 1
Day 21-42 Cluster 2
Day 21-42 Cluster 3
Proportion [%]
Ld QL9+ Day 0
Ld QL9+ Day 10
Ld QL9+ Day 21
Ld QL9+ Day 42
Bulk CD8+ Day 0
Bulk CD8+ Day 10
Bulk CD8+ Day 21
Bulk CD8+ Day 42
C
Day 10 Cluster 1
Day 10 Cluster 2
Day 10 Cluster 3
Day 10 Cluster 4
Day 21-42 Cluster 1
Day 21-42 Cluster 2
Day 21-42 Cluster 3
UMAP Dimension 1
UMAP Dimension 1
D
CD44
Ki67
CXCR3
CD62L
ICOS
KLRG-1
CD27
CD43
CD28
CD127
Average
Day 10 1
Day 10 2
Day 10 3
Day 10 4
Day 21-42 1
Day 21-42 2
Day 21-42 3
expression
E
CD44hi CD8+ T Cells Post-Graft
Day 0
Day 10
Day 21
Day 42
Bulk CD8+ T Cells
Ld QL9+ T Cells
CD62L
CD43
84.5
0.092
15.3
0.11
66.3
8.50
5.35
19.8
65.9
4.73
21.9
7.42
78.8
2.89
14.6
3.70
72.5
0.15
27.1
0.20
50.9
7.82
5.01
36.3
39.1
10.7
29.0
21.2
63.5
6.48
18.1
11.9
% CD62Llo CD43+
Bulk CD8+ T Cells
Ld QL9+ T Cells
% of Population
Day Post-Graft
0
10
21
42
60
40
20
0
**
*
**

Figure 6

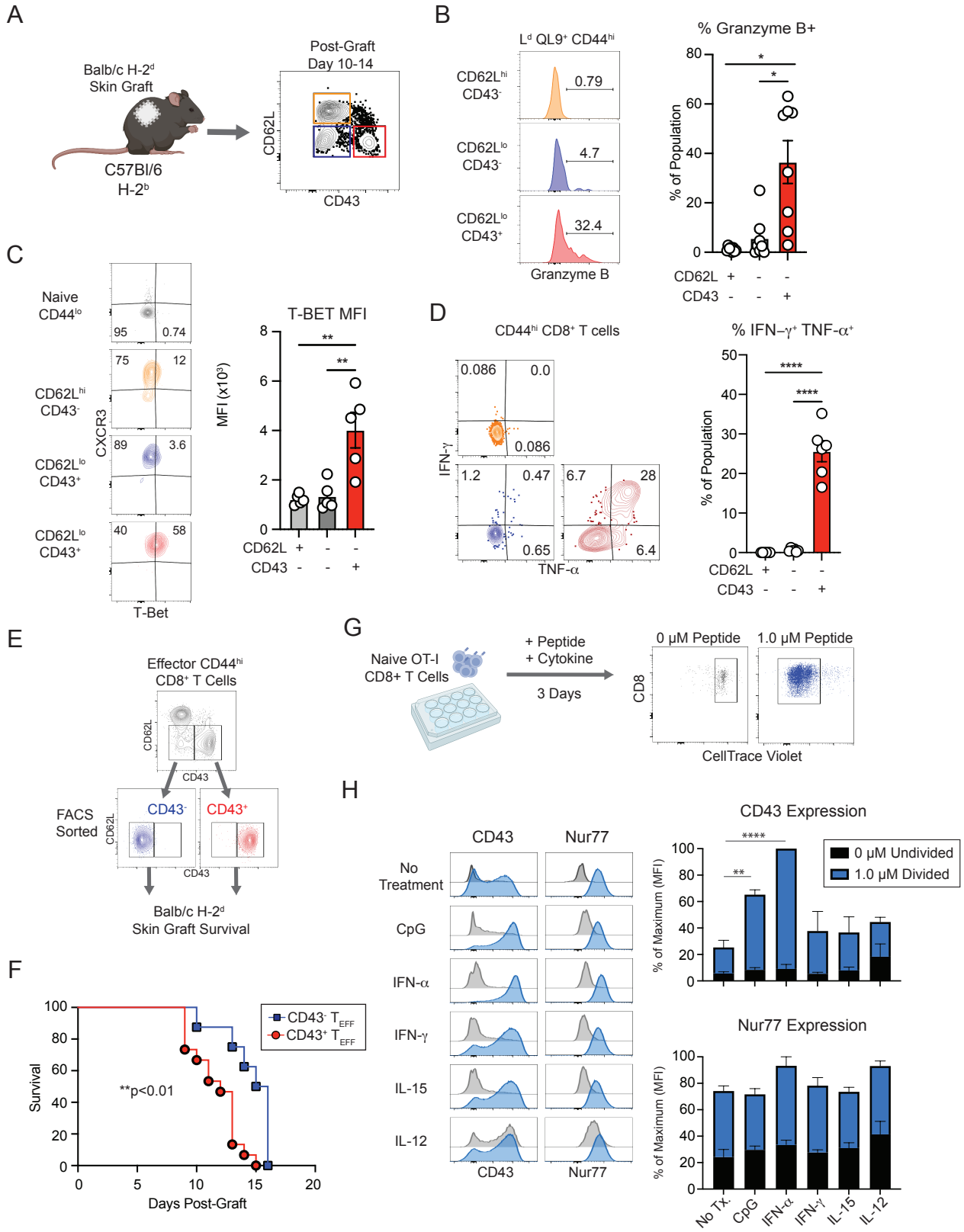
A
Balb/c H-2d
Skin Graft
C57Bl/6
H-2b
Post-Graft
Day 10-14
CD62L
CD43
B
Ld QL9+ CD44hi
CD62Lhi
CD43-
0.79
CD62Llo
CD43-
4.7
CD62Llo
CD43+
32.4
Granzyme B
% Granzyme B+
% of Population
CD62L + - -
CD43 - - +
C
Naive
CD44lo
95
0.74
CD62Lhi
CD43-
75
12
CD62Llo
CD43+
89
3.6
CD62Llo
CD43+
40
58
CXCR3
T-Bet
T-BET MFI
MFI (x10³)
CD62L + - -
CD43 - - +
D
CD44hi CD8+ T cells
0.086
0.0
0.086
1.2
0.47
0.65
6.7
28
6.4
IFN-γ
TNF-α
% IFN-γ+ TNF-α+
% of Population
CD62L + - -
CD43 - - +
E
Effector CD44hi
CD8+ T Cells
CD62L
CD43
FACS
Sorted
CD43-
CD43+
Balb/c H-2d
Skin Graft Survival
G
Naive OT-I
CD8+ T Cells
+ Peptide
+ Cytokine
3 Days
0 μM Peptide
1.0 μM Peptide
CD8
CellTrace Violet
H
CD43
Nur77
No
Treatment
CpG
IFN-α
IFN-γ
IL-15
IL-12
CD43 Expression
0 μM Undivided
1.0 μM Divided
% of Maximum (MFI)
Nur77 Expression
No Tx.
CpG
IFN-α
IFN-γ
IL-15
IL-12
F
Survival
**p<0.01
CD43- TEFF
CD43+ TEFF
Days Post-Graft

Figure 7

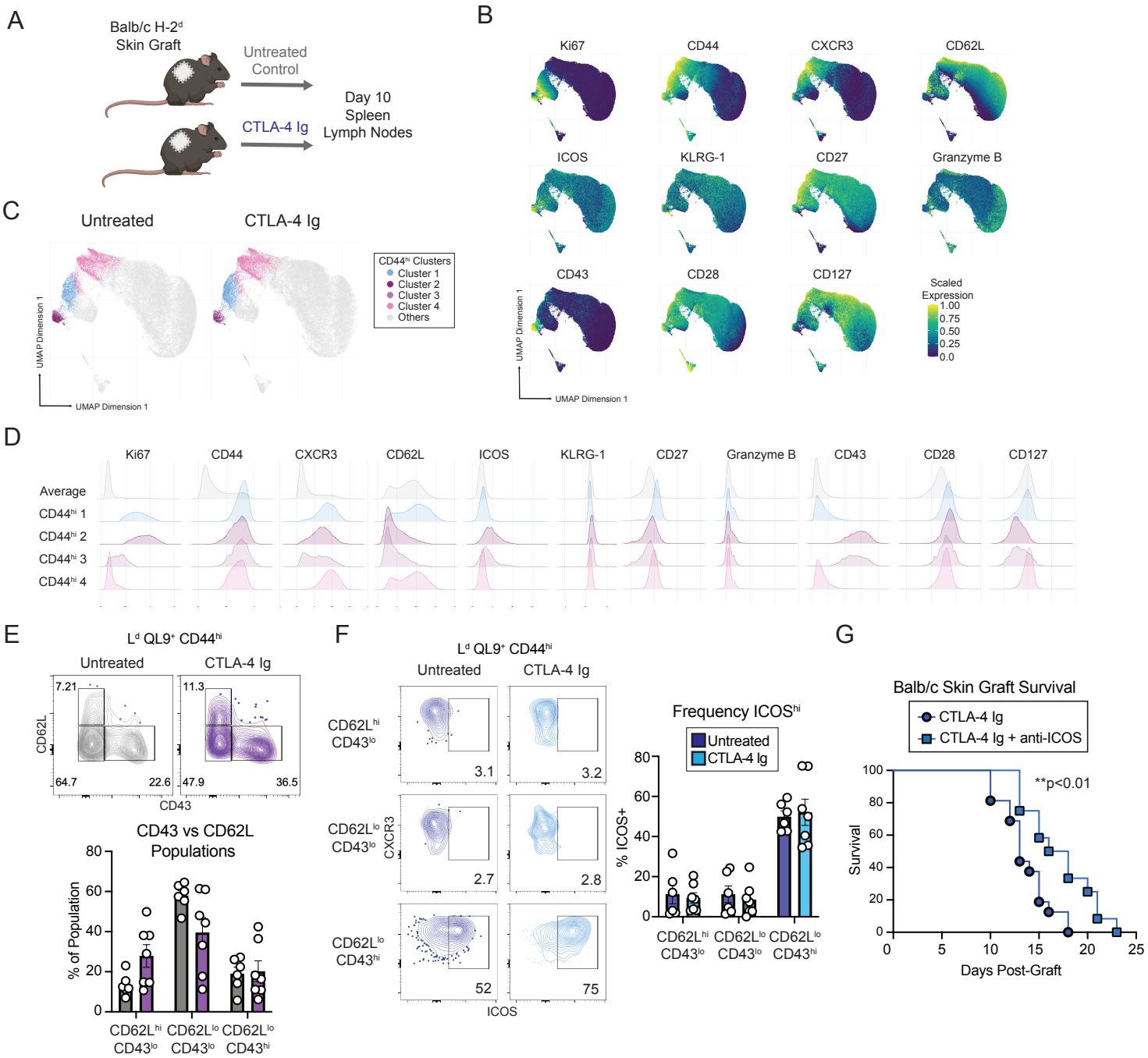
A
Balb/c H-2d
Skin Graft
Untreated
Control
CTLA-4 Ig
Day 10
Spleen
Lymph Nodes
B
Ki67
CD44
CXCR3
CD62L
ICOS
KLRG-1
CD27
Granzyme B
CD43
CD28
CD127
Scaled
Expression
1.00
0.75
0.50
0.25
0.0
UMAP Dimension 1
UMAP Dimension 1
C
Untreated
CTLA-4 Ig
CD44hi Clusters
Cluster 1
Cluster 2
Cluster 3
Cluster 4
Others
UMAP Dimension 1
UMAP Dimension 1
D
Ki67
CD44
CXCR3
CD62L
ICOS
KLRG-1
CD27
Granzyme B
CD43
CD28
CD127
Average
CD44hi 1
CD44hi 2
CD44hi 3
CD44hi 4
E
Ld QL9+ CD44hi
Untreated
CTLA-4 Ig
7.21
64.7
22.6
11.3
47.9
36.5
CD62L
CD43
CD43 vs CD62L
Populations
% of Population
80
60
40
20
0
CD62Lhi CD43lo
CD62Llo CD43lo
CD62Llo CD43hi
F
Ld QL9+ CD44hi
Untreated
CTLA-4 Ig
CD62Lhi
CD43lo
CD62Llo
CD43lo
CD62Llo
CD43hi
CXCR3
3.1
3.2
2.7
2.8
52
75
ICOS
Frequency ICOShi
Untreated
CTLA-4 Ig
% ICOS+
80
60
40
20
0
CD62Lhi CD43lo
CD62Llo CD43lo
CD62Llo CD43hi
G
Balb/c Skin Graft Survival
CTLA-4 Ig
CTLA-4 Ig + anti-ICOS
**p<0.01
Survival
100
80
60
40
20
0
0
5
10
15
20
25
Days Post-Graft

Figure S1

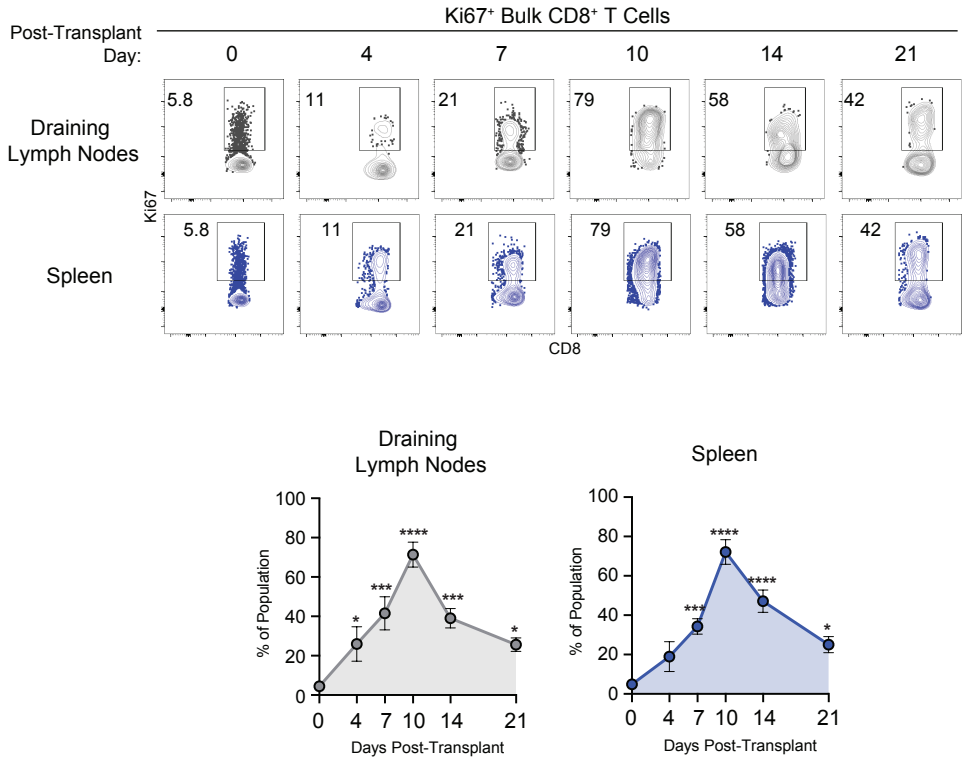
Ki67+ Bulk CD8+ T Cells
Post-Transplant Day:
0
4
7
10
14
21
Draining Lymph Nodes
Spleen
5.8
11
21
79
58
42
Ki67
CD8
Draining Lymph Nodes
Spleen
% of Population
Days Post-Transplant
0
20
40
60
80
100
*
***
****

Figure S2

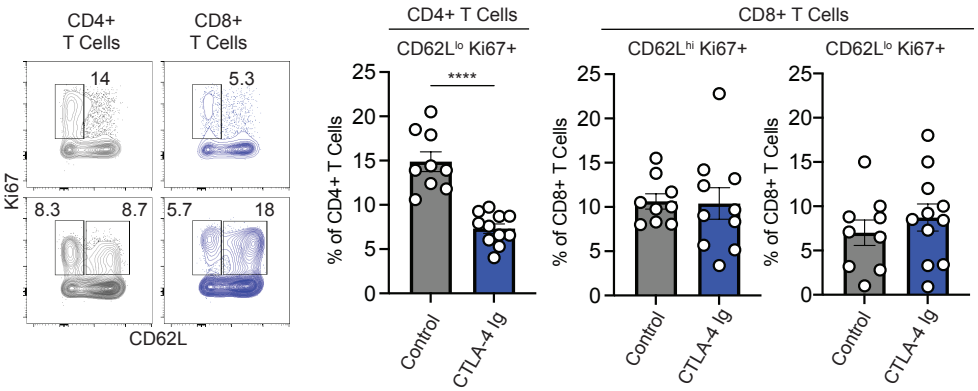
CD4+
T Cells
CD8+
T Cells
14
5.3
8.3
8.7
5.7
18
Ki67
CD62L
CD4+ T Cells
CD62L^{lo} Ki67+
****
% of CD4+ T Cells
Control
CTLA-4 Ig
CD8+ T Cells
CD62L^{hi} Ki67+
CD62L^{lo} Ki67+
% of CD8+ T Cells
Control
CTLA-4 Ig
% of CD8+ T Cells
Control
CTLA-4 Ig